electronics

MDPI

Article

A Unified Control and Fault Diagnosis Framework for Single-Area Load Frequency Control: Addressing Sensor Bias Fault Insensitivity in Integral Control Approaches

Ali M. H. Kadhim [1], Ahmed Al Ameri [1,*], Adnan Alamili [1] and Mamadou Baïlo Camara [2]

[1] Control and Management for Renewable Energy Research (CAMRERG), Electrical Engineering Department, University of Kufa, Najaf 31221, Iraq; alim.aljudi@uokufa.edu.iq (A.M.H.K.); adnan.alaamili@uokufa.edu.iq (A.A.)

[2] Groupe de Recherche en Electrotechnique et Automatique du Havre (GREAH), EA3220, Université Le Havre Normandie, 76600 Le Havre, France; camaram@univ-lehavre.fr

* Correspondence: ahmeds.alameri@uokufa.edu.iq

Abstract

This paper presents a unified control and fault diagnosis (UCFD) framework for single-area load frequency control (LFC) systems subject to load disturbances and sensor bias faults. Although integral-based LFC can eliminate steady-state frequency errors under nominal conditions, persistent sensor biases may be interpreted as genuine frequency deviations, resulting in erroneous control actions. To address this limitation, the proposed framework replaces integral action with a state-feedback and feedforward control structure and employs two dedicated observers: an augmented-state observer for reconstructing the system states and sensor bias as an additional state, and a residual-generation observer for generating a residual associated with load disturbances. By explicitly incorporating the measured load disturbance into the augmented observer, the proposed approach separates physical load variations from sensor-induced measurement errors and enables unbiased state reconstruction. The residual-generation observer, together with an auxiliary first-order compensator, is then used for load-disturbance rejection, while sensor bias accommodation is performed at the state-estimation level. An analytical expression for the compensator gain is derived from the steady-state disturbance-rejection condition, while its time constant is selected to provide appropriate separation between observer and compensation dynamics. The proposed framework is evaluated through four simulation cases involving load disturbances and sensor bias faults with different temporal profiles, including a combined scenario with model-parameter uncertainty and stochastic load demand. The results are compared with an integral state-feedback approach using frequency-regulation and control-effort metrics. Although integral control provides slightly better nominal performance, the proposed framework achieves substantially improved frequency regulation under faulty conditions and maintains zero steady-state frequency deviation in the presence of persistent sensor bias. Moreover, under faulty and uncertain conditions, the proposed framework reduces both the cumulative squared control effort and the peak control demand, demonstrating enhanced resilience to sensor-bias faults without imposing excessive actuator requirements.

Keywords: load frequency control (LFC); integral with state feedback control; unified control and fault diagnosis (UCFD) framework; load demands/disturbances; sensor bias faults

Check for updates

Academic Editor: Fernando Bento

Received: 3 October 2026
Revised: 21 October 2026
Accepted: 22 October 2026
Published: 27 October 2026

Copyright: © 2026 by the authors. Licensee MDPI, Basel, Switzerland. This article is an open access article distributed under the terms and conditions of the Creative Commons Attribution (CC BY) license.

1. Introduction

Modern electrical power grids require a continuous, real-time balance between total power generation and varying consumer load demands to maintain grid stability. Load frequency control (LFC) is the vital operational mechanism responsible for maintaining the system frequency within strict operational limits and regulating tie-line power exchanges in interconnected areas. If a severe load-generation mismatch occurs, the grid frequency deviates from its nominal value, which can trigger protective relays, damage synchronous generator turbines, and potentially escalate into cascading power blackouts. Consequently, developing robust, reliable, and highly responsive LFC frameworks has been a primary objective of power system engineering for decades, resulting in extensive academic reviews covering both classical and modern control methodologies [1,2].

The evolution of LFC from conventional techniques to advanced frameworks including fuzzy control, optimization strategies, and emerging challenges such as cyber-attacks and communication bandwidth constraints is comprehensively examined in [1]. Furthermore, a state-of-the-art review of LFC implementation in single-area and multi-area power systems highlighting the modern impacts of deregulation, distributed generation, and renewable energy integration on frequency stability is provided in [3]. Soft-computing-based approaches, encompassing fuzzy computing, evolutionary algorithms, swarm intelligence, and neural network hybrids for LFC modeling and optimization, are surveyed in [2], demonstrating their potential to enhance dynamic performance under system uncertainties.

To execute frequency regulation, power grids rely on a multi-layered hierarchical control architecture. Primary control utilizes local governor droop characteristics to instantly arrest sudden frequency drops, while secondary control (the primary domain of LFC) adjusts the generation set-points of dispatchable units to eliminate the remaining steady-state frequency error. Historically, this has been achieved using conventional proportional-integral (PI) loops. However, as modern grids encounter low-inertia conditions due to distributed energy integration, researchers have proposed more complex controlling strategies. Several studies have proposed novel meta-heuristic optimization algorithms for controller tuning, including [1,4–10], all demonstrating significant reductions in integral time absolute error (ITAE), frequency overshoot, and settling time. Complementing these efforts, intelligent learning-based frameworks have been extensively employed to enhance adaptability under system uncertainties, cyber-attacks, and varying weather conditions, as demonstrated in [11–13], which effectively limit frequency deviations without requiring prior system models. Advanced modeling and systematic control design frameworks are addressed in [14,15], while energy storage integration for frequency regulation is investigated in [16], where superconducting magnetic energy storage (SMES) is employed to improve dynamic frequency performance.

To further safeguard low-inertia grids against modern operational risks, robust sliding mode and adaptive controllers have been designed in [17–22]. Meanwhile, the authors in [14,16] integrated wind turbines (WTs), high-voltage direct current (HVDC) links, and battery energy storage systems (BESSs) with conventional synchronous generators to support inertia emulation. The integration of distributed energy resources and practical smart-grid applications is further highlighted in [8–10]. While these studies demonstrate a growing interest in intelligent frequency control frameworks, shifting toward data-driven and model-free paradigms [11,23–25], such methods often come with heavy computational overhead and lack explicit closed-loop deterministic stability proofs.

Furthermore, fractional-order and adaptive structures, such as the ANFIS and optimized variations presented in [4–6,17,26], focus heavily on mitigating generation and load uncertainties [13,14,18,19], yet they remain highly vulnerable to localized measurement anomalies. Even in studies addressing cybersecurity or communication delays through ro-

bust H_∞ frameworks [12,27], the emphasis is primarily placed on external data attenuation rather than internal sensor hardware vulnerabilities. Despite the sophistication of these advanced control strategies, a critical operational gap remains unaddressed.

Traditional and modern LFC frameworks alike rely fundamentally on integral feedback loops or direct tracking of measurement data to guarantee that the steady-state frequency error is driven to zero [28]. Although such frameworks are designed to reject external disturbances including stochastic load demand variations and unplanned generation imbalances, this operational dependency introduces a critical, hidden vulnerability: a susceptibility to both internal component failures and external adversarial disturbances.

Specifically, when a feedback sensor suffers a physical component failure, calibration drift, or a maliciously injected bias signal, the latter representing a form of adversarial cyber-attack targeting measurement integrity standard integral control loops cannot distinguish between a genuine external load disturbance and a corrupted internal measurement [29]. The controller therefore treats the erroneous sensor offset as a real power imbalance and, in attempting to force the faulty measurement to zero, inadvertently drives the actual physical system frequency away from its nominal value. This creates a dangerous artificial frequency deviation that originates not from any true external power imbalance but from the controller's own blind response to a corrupted internal signal—a vulnerability that remains entirely undetected and unmitigated by conventional integral-based LFC architectures. While the extensive literature focuses on handling external generation uncertainties, masking cyber-attacks, or minimizing communication transmission delays [12,26], there is a lack of simple, implementation-friendly structures capable of distinguishing an internal sensor fault from a true physical load change. To bridge this critical academic gap, this paper, inspired by [30], develops a unified control and fault diagnosis (UCFD) framework specifically for single-area LFC systems. Rather than relying on the Youla-parametrization technique in [30], the present study operates entirely within a practical, baseline state-space architecture. By combining state-feedback control with a residual generator loop and an auxiliary feedback controller Q, the framework detaches the error-rejection mechanism from direct sensor feedback tracking. As a result, the system achieves asymptotic rejection of physical step load disturbances while remaining insensitive to the onset of sudden step sensor biases. The performance is verified through comprehensive comparative simulation case studies.

The main novel contributions of this paper are summarized as follows:

1. The development of a unified control and fault diagnosis (UCFD) framework tailored specifically for single-area LFC systems, operating within a practical baseline state-space architecture without relying on complex Youla-parametrization.
2. The structural decoupling of sensor bias fault accommodation and load disturbance rejection, where the former is handled via an augmented-state observer and the latter via a residual-driven auxiliary compensator.
3. The derivation of explicit analytical expressions for the auxiliary compensator gain and time constant to guarantee zero steady-state frequency deviation under concurrent step load disturbances and persistent sensor biases.
4. A comprehensive comparative evaluation demonstrating that while conventional integral control blindly tracks corrupted measurements, the proposed UCFD framework maintains accurate regulation of the physical system frequency and significantly reduces peak control effort under faulty conditions.

The remainder of this article is organized as follows. Section 2 presents the mathematical model of the single-area LFC system. Section 3 investigates the performance of the conventional observer-based integral state-feedback control structure under various load disturbance and sensor fault scenarios, revealing its sensitivity to measurement bias.

Section 4 develops the proposed UCFD framework, including the augmented state estimator, state-feedback controller, feedforward reference-tracking mechanism, residual generator, and auxiliary compensation controller. In addition, explicit analytical expressions for the compensation gain and time constant are derived from the steady-state fault-accommodation requirements. Both Sections 3 and 4 conclude with simulation studies conducted under different disturbance and sensor fault conditions alongside model parameter uncertainty and stochastic load demand. Section 5 provides a quantitative evaluation of the obtained results, and Section 6 concludes the paper and discusses future research directions.

2. Modeling of Single-Area Load Frequency Control

The single-area load frequency control (LFC) model presented in this study integrates three fundamental subsystems: the speed governor, the turbine, and the generator-load assembly [31]. In power system dynamics, the frequency deviation ($\Delta\omega$) is the direct consequence of a real-power imbalance between the mechanical power supplied and the electrical load demand. Specifically, the discrepancy between the change in mechanical power (ΔP_m) and the change in load demand (ΔP_L) acts as a disturbance to the generator-load dynamics. In this work, ΔP_L is assumed to be a known, measured signal, which is realistic given modern phasor measurement unit (PMU) bus monitoring and enables precise controller performance evaluation [32].

Since significant deviations from the nominal frequency can compromise the stability, operational integrity, and efficiency of the power system, the control objective is to regulate $\Delta\omega$ toward zero. This is achieved through a primary control loop that monitors the generator speed deviations and feeds the signal back via a speed regulation constant ($1/R$); see Figure 1. This feedback is compared against the reference power (ΔP_{ref}), prompting the governor to adjust the valve position (ΔP_V). This adjustment alters the mechanical power (ΔP_m) to compensate for load changes and restore the frequency to its normal value [33].

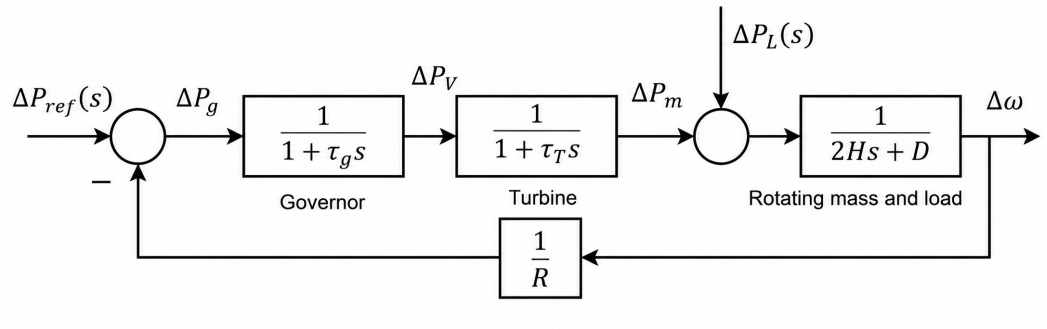


Figure 1. Load frequency control block diagram of a single area.

From the transfer functions of the governor, turbine, and generator-load assembly as shown in Figure 1, the system dynamics are initially governed by

$$(1 + \tau_g s)\Delta P_V(s) = \Delta P_{ref}(s) - \frac{1}{R}\Delta\omega(s) \quad (1)$$

$$(1 + \tau_T s)\Delta P_m(s) = \Delta P_V(s) \quad (2)$$

$$(2Hs + D)\Delta\omega(s) = \Delta P_m(s) - \Delta P_L(s) \quad (3)$$

where τ_g and τ_T are the time constants of the governor and turbine, respectively, H is the inertia constant, and D represents the damping coefficient [31,34].

By solving for the first-order derivative terms, the equations are rearranged as follows

$$s\Delta P_V(s) = -\frac{1}{\tau_g}\Delta P_V(s) - \frac{1}{R\tau_g}\Delta\omega(s) + \frac{1}{\tau_g}\Delta P_{ref}(s) \tag{4}$$

$$s\Delta P_m(s) = \frac{1}{\tau_T}\Delta P_V(s) - \frac{1}{\tau_T}\Delta P_m(s) \tag{5}$$

$$s\Delta\omega(s) = \frac{1}{2H}\Delta P_m(s) - \frac{D}{2H}\Delta\omega(s) - \frac{1}{2H}\Delta P_L(s) \tag{6}$$

By defining the state vector $\mathbf{x} = [\Delta P_V \quad \Delta P_m \quad \Delta\omega]^T$, the control input $u(t) = \Delta P_{ref}$, and the disturbance $d(t)$ equals the load demand ΔP_L, and by considering $\Delta\omega$ is the only measured output, the system can be represented in a compact state-space form as

$$\dot{\mathbf{x}}(t) = \mathbf{A}\mathbf{x}(t) + \mathbf{B}u(t) + \mathbf{B_d}d(t) \tag{7}$$

$$y = \mathbf{C}\mathbf{x}(t) \tag{8}$$

where the full state-space form is as follows (t is dropped for simplicity and will be used whenever necessary):

$$\overbrace{\begin{bmatrix}\Delta\dot{P}_V\\ \Delta\dot{P}_m\\ \Delta\dot{\omega}\end{bmatrix}}^{\dot{\mathbf{x}}} = \overbrace{\begin{bmatrix}-\frac{1}{\tau_g} & 0 & -\frac{1}{R\tau_g}\\ \frac{1}{\tau_T} & -\frac{1}{\tau_T} & 0\\ 0 & \frac{1}{2H} & -\frac{D}{2H}\end{bmatrix}}^{\mathbf{A}}\overbrace{\begin{bmatrix}\Delta P_V\\ \Delta P_m\\ \Delta\omega\end{bmatrix}}^{\mathbf{x}} + \overbrace{\begin{bmatrix}\frac{1}{\tau_g}\\ 0\\ 0\end{bmatrix}}^{\mathbf{B}}\overbrace{\Delta P_{ref}}^{u} + \overbrace{\begin{bmatrix}0\\ 0\\ -\frac{1}{2H}\end{bmatrix}}^{\mathbf{B_d}}\overbrace{\Delta P_L}^{d} \tag{9}$$

$$y = \overbrace{\begin{bmatrix}0 & 0 & 1\end{bmatrix}}^{\mathbf{C}}\begin{bmatrix}\Delta P_V\\ \Delta P_m\\ \Delta\omega\end{bmatrix} \tag{10}$$

For small frequency deviations, the aforementioned primary control loop is sufficient to restore the frequency to its nominal value. However, for larger deviations, an additional control loop with integral action is typically incorporated into the LFC, as discussed in the following section.

3. Integral Reference Tracking with State-Feedback Control

Although PI controllers are widely employed in LFC due to their simplicity and ability to eliminate steady-state frequency deviations, their performance is limited to shaping the output system dynamics. To overcome these limitations, a state-feedback control approach based on pole-placement is adopted to achieve the desired transient performance through full state utilization. An integral action is further incorporated into the state feedback structure to ensure zero steady-state error under load disturbances, resulting in a more effective frequency regulation strategy [31].

This approach requires selecting two gains, integral gain (K_I) for reference tracking and state-feedback gain ($\mathbf{K}_0$) to get satisfactory dynamic response of states during disturbance rejection, see Figure 2. The mentioned gains can be determined through different techniques, yet the pole-placement technique is employed in this work. However, selecting $\mathbf{K}_0$ assumes that all system state variables are measured and available to be used in feedback [31,35]. In most cases, this is not possible for different reasons, e.g., prohibitive sensor usage, excessive measurement noise or unmeasurable states. Thus, a state estimator is to be designed to re-construct the state variables and feed them back through ($\mathbf{K}_0$) to the system, as detailed in the following sections.

3.1. Full-State Estimator

Because measurements of all state variables are not always available in practice, the implementation of state-feedback control requires a state estimator to reconstruct the system state variables from available measurements. This enables the practical realization of the proposed control scheme while maintaining the desired dynamic performance [35].

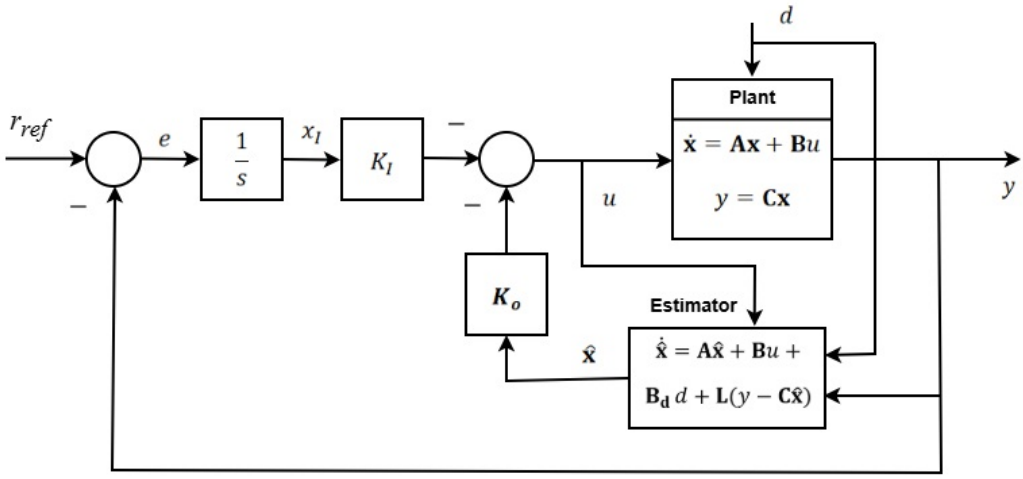


Figure 2. Integral control with state-feedback control and state estimator.

A state estimate ($\hat{\mathbf{x}}$) of a system

$$\dot{\mathbf{x}} = \mathbf{A}\mathbf{x} + \mathbf{B}u + \mathbf{B_d}d \tag{11}$$

$$y = \mathbf{C}\mathbf{x} \tag{12}$$

excited by $u(t)$, can be obtained through an estimator model

$$\dot{\hat{\mathbf{x}}} = \mathbf{A}\hat{\mathbf{x}} + \mathbf{B}u + \mathbf{B_d}d + \mathbf{L}(y - \mathbf{C}\hat{\mathbf{x}}) \tag{13}$$

where $\mathbf{L}$ is a proportional gain determined to drive the state-estimate error ($\tilde{\mathbf{x}} = \mathbf{x} - \hat{\mathbf{x}}$) to zero [35,36]. The estimation error dynamics are obtained by subtracting (11) from (13) and substituting y with (12), yielding

$$\dot{\tilde{\mathbf{x}}} = (\mathbf{A} - \mathbf{LC})\tilde{\mathbf{x}} \tag{14}$$

Thus, $\tilde{\mathbf{x}}(t) = e^{-(\mathbf{A}-\mathbf{LC})t}\tilde{\mathbf{x}}(0)$ will decay to zero regardless of the initial estimation error $\tilde{\mathbf{x}}(0)$, if $\mathbf{L}$ is selected by means of the pole-placement technique, so the eigenvalues of $(\mathbf{A} - \mathbf{LC})$ are stable and reasonably fast [35,36]. It is worth noting that to ensure the augmented observer yields unbiased and accurate state estimates, the measured load demand $d = \Delta P_L$ is explicitly incorporated as a known input into the observer dynamics via the distribution matrix $\mathbf{B_d}$. This design choice is critical to prevent the observer from misinterpreting the physical steady-state frequency deviation caused by the load as an unmodeled disturbance. By explicitly accounting for the known physical disturbance, the augmented observer accurately isolates the true unknown fault while maintaining pristine state estimates. Consequently, this enables the generation of a cleaned measurement signal, ensuring that the downstream nominal observer and residual generator operate on uncompromised data.

3.2. State-Feedback and Integral Reference Tracking Control Law

For the linear system in (11) and (12), the state-feedback control law

$$u = -\mathbf{K}_0\mathbf{x} \tag{15}$$

stabilizes the system and regulates the state toward its equilibrium point, provided that the eigenvalues of $(\mathbf{A} - \mathbf{BK}_0)$ are properly assigned [35]. However, considering the LFC system in (7) and (8), which is subject to persistent external disturbance (d) and with the objective of driving the output $y = \Delta\omega$ to zero, the state-feedback control (15) is generally insufficient to eliminate the steady-state error.

To eliminate the steady-state error, a reference signal $r_{ref} = \Delta\omega_{ref}$ is introduced and the tracking error is defined as $e = y - r_{ref}$. Integral action is then incorporated by augmenting the state of the system with an additional state (x_I) corresponding to the integral of the tracking error as

$$x_I = \int^t e(\tau)d\tau \tag{16}$$

Hence, the state-feedback control law becomes

$$u = -K_I x_I - \mathbf{K_0 x} \tag{17}$$

where K_I and $\mathbf{K_0}$ are the integral and state-feedback gains, respectively. The gains K_I and $\mathbf{K_0}$ are obtained using pole-placement applied to the augmented system consisting of the system dynamics and the integral-state dynamics ($\dot{x}_I = \mathbf{Cx} - r_{ref}$) as

$$\begin{bmatrix} \dot{x}_I \\ \dot{\mathbf{x}} \end{bmatrix} = \overbrace{\begin{bmatrix} 0 & \mathbf{C} \\ 0 & \mathbf{A} \end{bmatrix}}^{\mathbf{A_c}} \overbrace{\begin{bmatrix} x_I \\ \mathbf{x} \end{bmatrix}}^{\mathbf{x_c}} + \overbrace{\begin{bmatrix} 0 \\ \mathbf{B} \end{bmatrix}}^{\mathbf{B_c}} u - \begin{bmatrix} 1 \\ \mathbf{0} \end{bmatrix} r_{ref} + \begin{bmatrix} 0 \\ \mathbf{B_d} \end{bmatrix} d \tag{18}$$

where, in the context of the LFC system,

$$\mathbf{A_c} = \begin{bmatrix} 0 & 0 & 0 & 1 \\ 0 & -\frac{1}{\tau_g} & 0 & -\frac{1}{R\tau_g} \\ 0 & \frac{1}{\tau_T} & -\frac{1}{\tau_T} & 0 \\ 0 & 0 & \frac{1}{2H} & -\frac{D}{2H} \end{bmatrix}, \mathbf{B_c} = \begin{bmatrix} 0 \\ \frac{1}{\tau_g} \\ 0 \\ 0 \end{bmatrix} \text{ and } \mathbf{x_c} = \begin{bmatrix} x_I \\ \Delta P_V \\ \Delta P_m \\ \Delta\omega \end{bmatrix} \tag{19}$$

Finally, the integral state-feedback control law of (17) can be written in a compact form as

$$u = -\overbrace{\begin{bmatrix} K_I & \mathbf{K_0} \end{bmatrix}}^{\mathbf{K_c}} \begin{bmatrix} x_I \\ \mathbf{x} \end{bmatrix} \tag{20}$$

It is worth noting the following:

1. Because the state-feedback controller in (15) uses the estimated state variables ($\hat{\mathbf{x}}$), u is reformulated as $u = -\mathbf{K_0}\hat{\mathbf{x}}$, see Figure 2.
2. In the same context, since x_I is defined as the integral of the tracking error ($\Delta\omega - \Delta\omega_{\text{ref}}$), it uses measured output $y = \Delta\omega_m$ rather than the estimated $\Delta\hat{\omega}$, as illustrated in the Figure 2. This is because the integral action accumulates any bias present in $\Delta\hat{\omega}$, particularly during the transient phase before convergence, which may lead to incorrect control action even after the state estimate has converged to its true value.
3. The guidelines for selecting appropriate eigenvalues of ($\mathbf{A - LC}$) and ($\mathbf{A_c - B_c K_c}$), which determine the observer gain $\mathbf{L}$ and controller gain $\mathbf{K_c}$, are beyond the scope of this article and can be found in standard control theory textbooks, e.g., [35,36]. As a general design guideline, the observer dynamics are chosen to be faster than the controller dynamics to ensure adequate state estimation performance. Accordingly, in this work, the observer eigenvalues are placed approximately five times farther into the left-half plane than the LFC system eigenvalues ($eig(\mathbf{A})$), while the controller eigenvalues are placed approximately three times farther than $eig(\mathbf{A})$, as implemented using MATLAB pole-placement routines.

3.3. Simulation Case Study 1

The frequency-regulation performance under an integral with state-feedback control scheme is evaluated for an isolated 1000-MVA reheat thermal steam turbine-generator power station subjected to a sudden load change of $\Delta P_L = 0.2$ p.u. The system is modeled using the standard parameters listed in Table 1, which are widely adopted as a benchmark

for single-area load frequency control (LFC) studies in power-system engineering [31,33]. The power station is characterized by the following parameters

Table 1. Parameters of a single-area power system.

Parameter	Value
Speed regulation	$R = 0.05$
Frequency-sensitive load coefficient	$D = 0.6$
Inertia constant	$H = 5$
Base power	1000 MVA
Governor time constant	$\tau_g = 0.2$ s
Turbine time constant	$\tau_T = 0.5$ s

By substituting the parameters of the power system in LFC state-space model of (9) and (10), the matrices

$$\mathbf{A} = \begin{bmatrix} -5 & 0 & -100 \\ 2 & -2 & 0 \\ 0 & 0.1 & -0.06 \end{bmatrix}, \quad \mathbf{B} = \begin{bmatrix} 5 \\ 0 \\ 0 \end{bmatrix}, \quad \mathbf{B_d} = \begin{bmatrix} 0 \\ 0 \\ -0.1 \end{bmatrix} \quad \mathbf{C} = \begin{bmatrix} 0 & 0 & 1 \end{bmatrix}$$

are obtained under the assumption that only the frequency deviation ($\Delta\omega$) is measured.

Determining $\mathbf{L}$ is needed to estimate the system state by employing the estimator model (13). As mentioned before, this can be done using the pole-placement technique through the MATLAB command `place` after substituting $\mathbf{A}^T$, $\mathbf{C}^T$, and selected eigenvalues, where T is the matrix transpose. For the following eigenvalues

$$-29.42, \quad -2.939 \pm 2.88i,$$

selected as $5 \times eig(\mathbf{A})$ with tuning of the imaginary values, the outcome of `place` routine is

$$\mathbf{L} = 10^2 \times \begin{bmatrix} 143.11 \\ -1.819 \\ 0.282 \end{bmatrix}$$

In a similar manner, $\mathbf{K_c}$ is obtained using `place` command after substituting proper selected eigenvalues with $\mathbf{A_c}$ and $\mathbf{B_c}$ of (19). Thus, for the eigenvalues

$$-17.6523, \quad -1.7638 \pm 5.3289i, \quad -5$$

selected as $3 \times eig(\mathbf{A})$ in addition to -5 for augmenting the integral state x_I, the outcome of `place` function is

$$\mathbf{K_c} = 10^3 \times \begin{bmatrix} 2.7810 & 0.0038 & 0.0150 & 0.9932 \end{bmatrix}$$

After determining $\mathbf{L}$ and $\mathbf{K_c}$, LFC under integral and state-feedback control is implemented using the MATLAB R2018b/Simulink package.

In the following, three cases are studied:

Case 1 simulates the system response to a load demand of $\Delta P_L = 0.2$ p.u. at 15 s as shown in Figure 3. Figure 3a–c demonstrate the state variables (ΔP_v, ΔP_m, and $\Delta\omega$) with the estimated ones ($\Delta\hat{P}_v$, $\Delta\hat{P}_m$ and $\Delta\hat{\omega}$), while the disturbance ΔP_L is in Figure 3d. The results demonstrate the effectiveness of the integral reference tracking with state-feedback control in the LFC system.

From an estimation perspective, the estimated variables closely track the actual ones, indicating accurate observer performance with fast convergence and negligible steady-state estimation error. Minor deviations during the transient phase are observed but quickly diminish, confirming the proper selection of observer dynamics.

From a control perspective, the system exhibits a well-damped response following the load disturbance applied at $t = 15$ s. The frequency deviation $\Delta\omega$ is effectively regulated and returns to zero (with approximately 3 s settling time), validating the capability of the integral action to eliminate steady-state error. Additionally, the control input (ΔP_v) and mechanical power (ΔP_m) responses remain bounded and settled smoothly, confirming the effectiveness of this approach to handle the load demand.

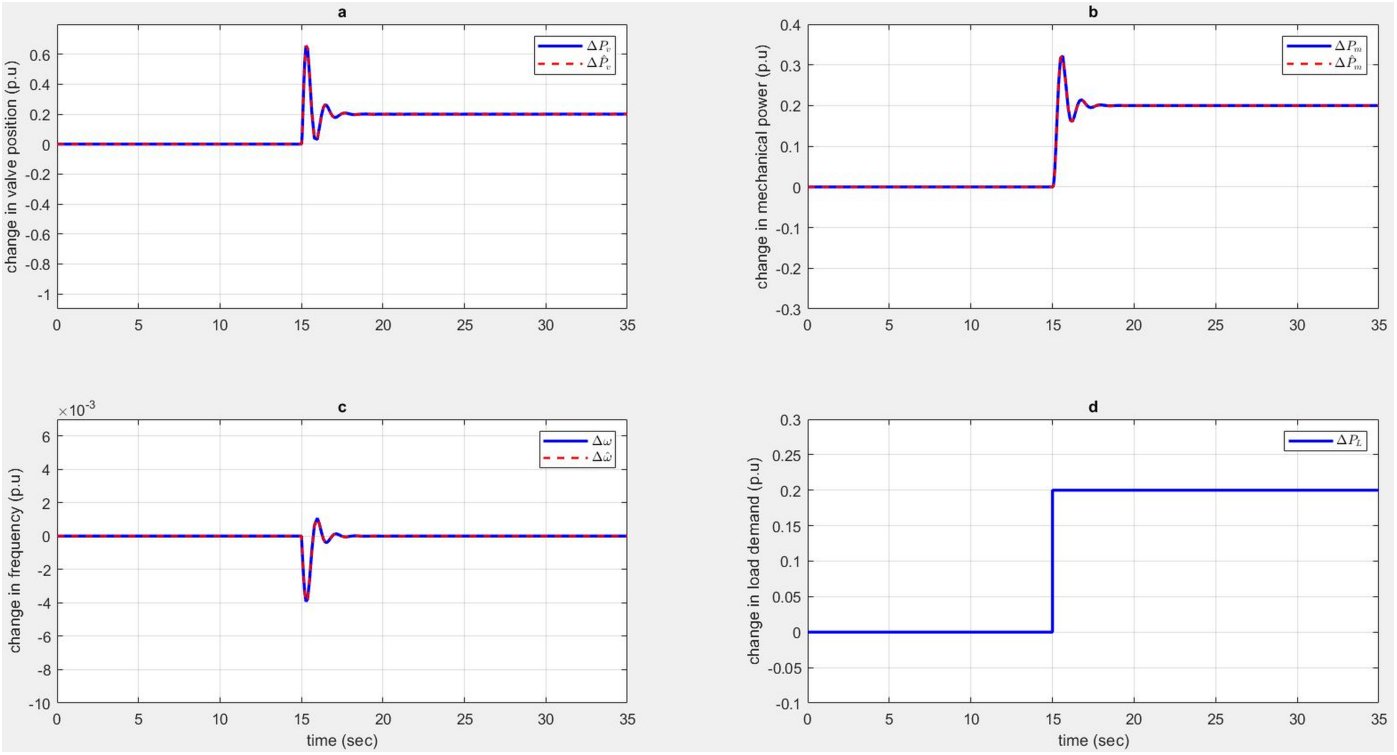


Figure 3. Response of the LFC system under integral with state-feedback control for $\Delta P_L = 0.2$ p.u. at 15 s: (**a**) change in valve position, (**b**) change in mechanical power, (**c**) change in frequency, and (**d**) change in load demand.

Cases 2 and 3 simulate the system response to a load demand of $\Delta P_L = 0.2$ p.u. at 15 s with a sensor bias fault assumed at 25 s and 5 s, respectively. The sensor bias fault (also referred to as a sensor offset) is among common faults encountered in the practice and modeled as an additive constant [37], see Figure 4.

In this work, the sensor fault is simulated by adding $f_s = 0.005$ p.u to the y measurement at the mentioned times, hence, in Case 2 , y at $t \geq 25$ s becomes

$$y = \mathbf{Cx} + f_s = \Delta\omega_m = \Delta\omega + f_s \tag{21}$$

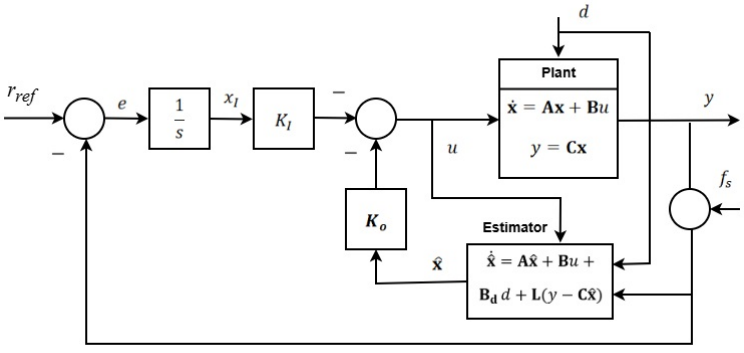


Figure 4. Simulation of the sensor bias fault.

Figure 5 illustrates the real and the estimated state variables affected by the load demand at 15 s and the sensor bias fault at 25 s as well as the measured change in the frequency ($\Delta\omega_m$). The response of the LFC is similar to the response of Case 1 up to $t < 25$ s; thereafter, one can notice two clear problems:

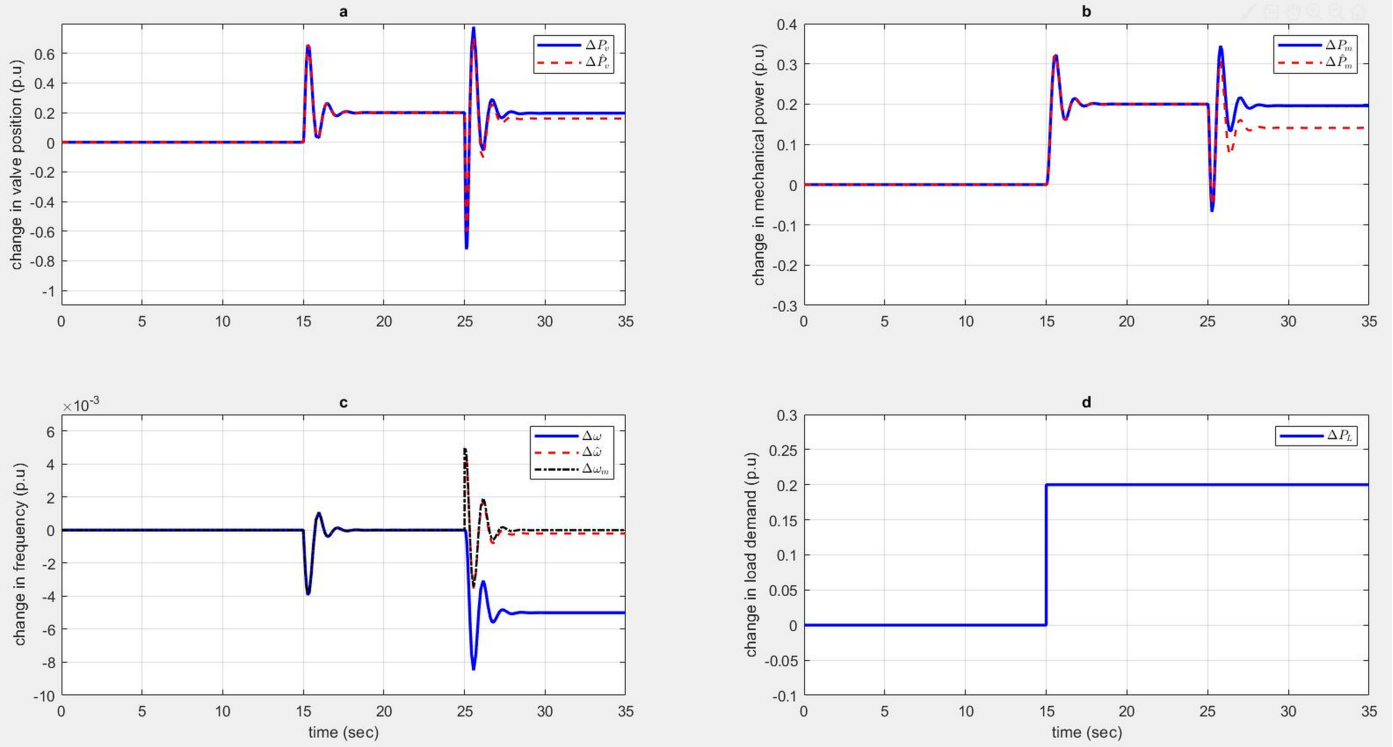


Figure 5. Response of the LFC system under integral with state-feedback control for $\Delta P_L = 0.2$ p.u. at 15 s with sensor bias fault of $f_s = 0.005$ p.u. for $t \geq 25$ s: (**a**) change in valve position, (**b**) change in mechanical power, (**c**) change in frequency, and (**d**) change in load demand.

1. A clear steady-state estimation error of the state variables ($\hat{\mathbf{x}}$) after the transient phase has elapsed. The steady-state estimation error ($\tilde{\mathbf{x}}(\infty)$) in all $\hat{\mathbf{x}}$ variables can be determined as

$$\tilde{\mathbf{x}}(\infty) = (\mathbf{A} - \mathbf{LC})^{-1}\mathbf{L}f_s \tag{22}$$

Hence, after substituting the values of $\mathbf{A}, \mathbf{L}, \mathbf{C}$, and f_s in (22), $\tilde{\mathbf{x}}(\infty)$ returns

$$\tilde{\mathbf{x}}(\infty) = \begin{bmatrix} \Delta\tilde{P}_v \\ \Delta\tilde{P}_m \\ \Delta\tilde{\omega} \end{bmatrix} = \begin{bmatrix} 0.0367 \\ 0.0555 \\ -0.0048 \end{bmatrix}$$

which is confirmed by the corresponding sub-plots in Figure 5.

2. More importantly, and directly related to the objective of this work, the behavior of the conventional integral control approach under this scenario reveals a fundamental limitation. Following the application of the sensor bias f_s at $t = 25$ s, the measured frequency deviation exhibits an additive 0.005 p.u. offset at fault onset. The integral controller responds to this biased measurement and drives the measured frequency deviation back to zero, thereby eliminating the apparent steady-state error while failing to recognize that the actual frequency deviation $\Delta\omega$ remains biased by -0.005 p.u., as shown in Figure 5c. Consequently, the controller achieves zero error with respect to the corrupted measurement rather than the actual system frequency. The figure also shows that the estimated frequency deviation $\Delta\hat{\omega}$ settles at approximately -0.0002 p.u. as explained in the former point. This behavior

is expected because the conventional integral controller relies directly on the measured tracking error and has no mechanism for detecting or accommodating sensor faults. Hence, despite eliminating the apparent steady-state error, the integral controller remains insensitive to the presence of the sensor bias and cannot guarantee accurate regulation of the actual system frequency.

Case 3 illustrates more severe scenario in which the sensor fault occurred before a change in load demand; see Figure 6. Similar problems with frequency regulation are observed, see Figure 6a, and hence a framework addresses the insensitivity of the sensor bias fault is required.

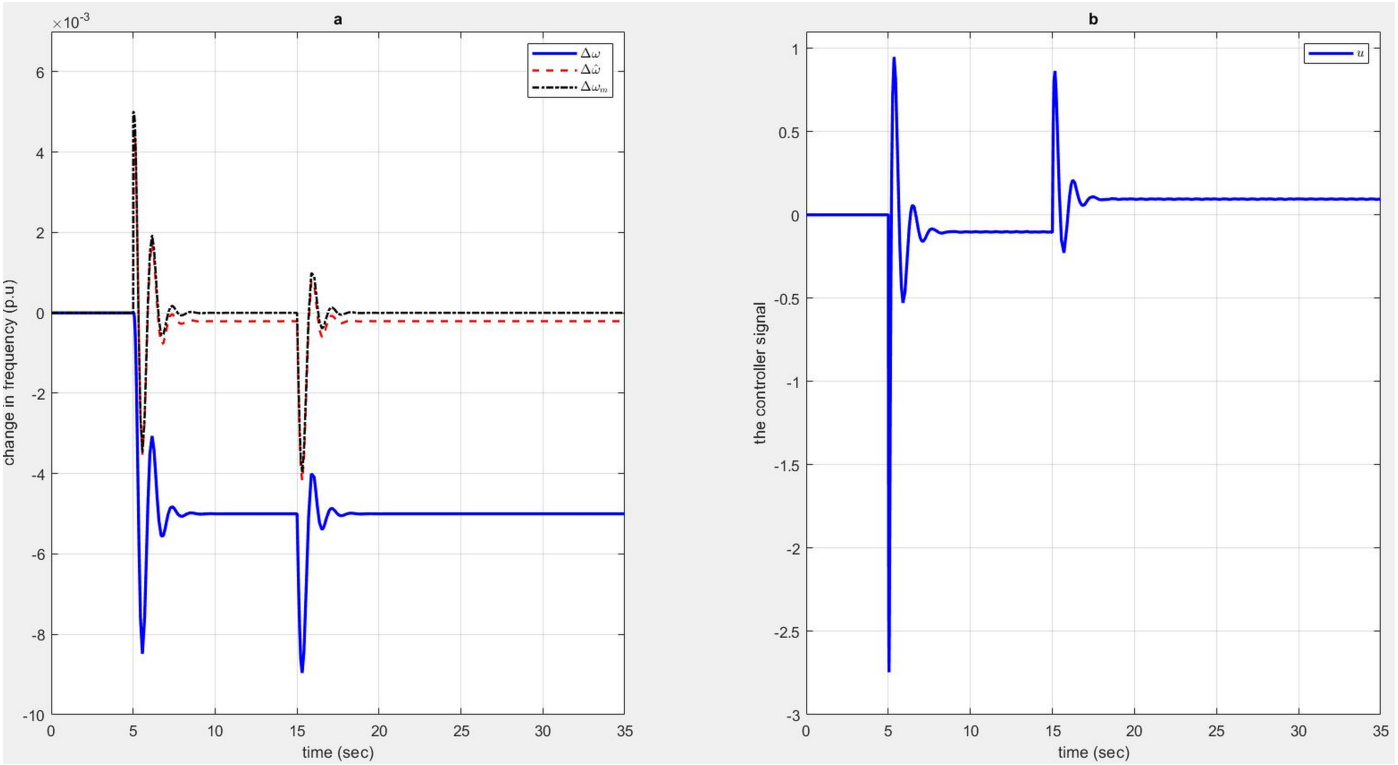


Figure 6. Response of the LFC system under integral with state-feedback control for $\Delta P_L = 0.2$ p.u. at 15 s with sensor bias fault of $f_s = 0.005$ p.u. for $t \geq 5$ s: (**a**) change in frequency and (**b**) the controller signal.

Figure 6b illustrates the dynamic response of the control signal $u(t)$ under sequential disturbance events. At $t = 5$ s, the sudden occurrence of a positive sensor bias fault (f_s) induces an immediate, high-magnitude negative transient spike in $u(t)$, dropping sharply to -2.75 p.u. As the integral loop acts on the corrupted measurement, $u(t)$ stabilizes at a negative baseline to counteract the apparent over-frequency. Upon the application of the load demand step $\Delta P_L = 0.2$ p.u. at $t = 15$ s, $u(t)$ exhibits a characteristic positive control effort spike, eventually settling at a positive steady-state value of 0.1 p.u. to maintain continuous power equilibrium.

Case 4 aims to assess the robustness of the integral control approach under realistic operating conditions. The system is evaluated in the presence of simultaneous parameter uncertainty, stochastic load fluctuations, and a persistent sensor-bias fault. Accordingly, the physical plant parameters are perturbed to represent moderate modeling uncertainty, with the damping coefficient D, inertia constant H, and governor time constant τ_g increased by 15%, 10%, and 5%, respectively. The load disturbance is represented as

$$\Delta P_L(t) = \Delta P_{L,\text{step}}(t) + \delta \Delta P_L(t),$$

where a deterministic load step of $\Delta P_{L,\text{step}}(t) = 0.2$ p.u. is applied at $t = 15$ s, while $\delta\Delta P_L(t)$ represents continuous stochastic load fluctuations modeled as a filtered zero-mean random process corresponding to 10 MW variation on a 1000-MVA base. In addition, a persistent sensor bias fault of $f_s = 0.005$ p.u. is introduced at $t = 5$ s.

The resulting responses are shown in Figure 7. As illustrated in Figure 7a, the sensor bias fault introduced at $t = 5$ s produces an immediate positive shift in the measured frequency $\Delta\omega_m$. Since the integral controller responds only to the measured frequency error, it interprets this measurement bias as a genuine frequency deviation and continues to act until the corrupted measurement is driven toward zero. Consequently, although $\Delta\omega_m$ is regulated close to zero, the actual physical frequency $\Delta\omega$ settles at approximately -0.005 p.u. This clearly illustrates the fundamental limitation of integral action in the presence of a persistent sensor bias: eliminating the measured steady-state error does not necessarily imply elimination of the actual physical frequency deviation.

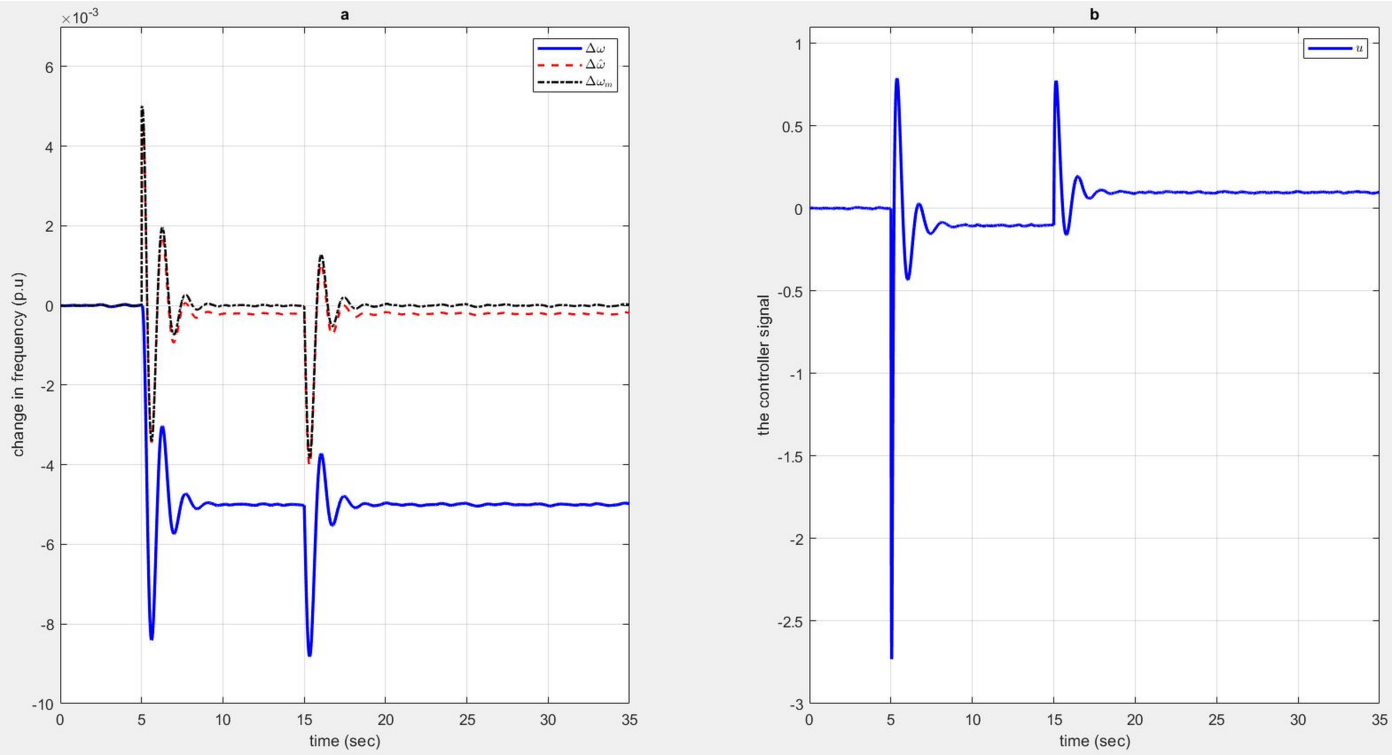


Figure 7. Response of the LFC system under integral control with state feedback for $\Delta P_{L,\text{step}} = 0.2$ p.u. at 15 s and a sensor-bias fault of $f_s = 0.005$ p.u. for $t \geq 5$ s: (**a**) change in frequency and (**b**) the controller signal.

The stochastic component of the load disturbance introduces persistent fluctuations into the frequency responses. These fluctuations are superimposed on the biased operating condition, while the parameter perturbations further represent the mismatch between the controller design model and the actual plant dynamics. Thus, the integral controller simultaneously compensates for the physical load disturbance and the erroneous measurement bias, without having the information required to distinguish between the two effects.

The corresponding control signal $u(t)$ is shown in Figure 7b. The introduction of the sensor bias at $t = 5$ s produces a pronounced negative transient, reaching approximately -2.7 p.u. This is followed by another significant transient in response to the 0.2 p.u. load step at $t = 15$ s. More importantly, after the transients decay, the control input settles around approximately 0.1 p.u., rather than the 0.2 p.u. level associated with the physical load change. This offset reflects the fact that part of the control action is continuously devoted to

compensating for the sensor-induced error. The stochastic load component and parameter mismatch also result in persistent fluctuations in the control signal.

Overall, Case 4 demonstrates that the integral control structure becomes unable to distinguish a persistent measurement error from an actual frequency deviation. Consequently, it regulates the corrupted measurement rather than the physical frequency, resulting in a nonzero steady-state frequency bias and substantial transient control effort. The results therefore highlight the sensitivity of the integral control approach to sensor bias faults, particularly when model uncertainty and stochastic load variations are simultaneously present.

4. Unified Control and Fault Diagnosis Framework

The UCFD framework implemented in this article is inspired by [30,37], which introduce a unified approach that integrates control and detection, extending existing methods used in fault diagnosis, fault-tolerant control, and performance degradation detection and recovery. However, unlike these works, which rely on the Youla-parameterization technique, the present study adopts a more conventional observer-based design for its structural transparency and ease of tuning, making it more suitable for practical implementation in LFC systems.

The UCFD framework differs fundamentally from the aforementioned integral-tracking state-feedback approach. Although both approaches employ state-feedback control in conjunction with a state estimator to regulate the system dynamics, the proposed UCFD framework explicitly augments the sensor-bias fault f_s as an additional state within the estimator. This reformulation transforms f_s from an unmodeled measurement uncertainty into an endogenous state variable that can be dynamically reconstructed. Consequently, the augmented estimator can asymptotically recover both the original system state $\mathbf{x}$ and the sensor-bias magnitude f_s, thereby driving the estimation error toward zero and eliminating the steady-state state-estimation bias induced by the sensor fault.

Furthermore, rather than relying on integral action, the proposed framework employs a feedforward controller K_F, together with a residual generator and an auxiliary feedback compensator Q, primarily to reject load disturbances ΔP_L, as illustrated in Figure 8. Accordingly, the roles of sensor-fault accommodation and disturbance rejection are explicitly separated: the former is addressed through augmented state estimation and reconstruction of f_s, whereas the latter is handled through residual-driven feedback compensation. This configuration enables reference tracking, load-disturbance rejection, and sensor-fault accommodation to be addressed through dedicated mechanisms, while avoiding the inherent limitations associated with the accumulation of biased tracking errors in the integral control approach.

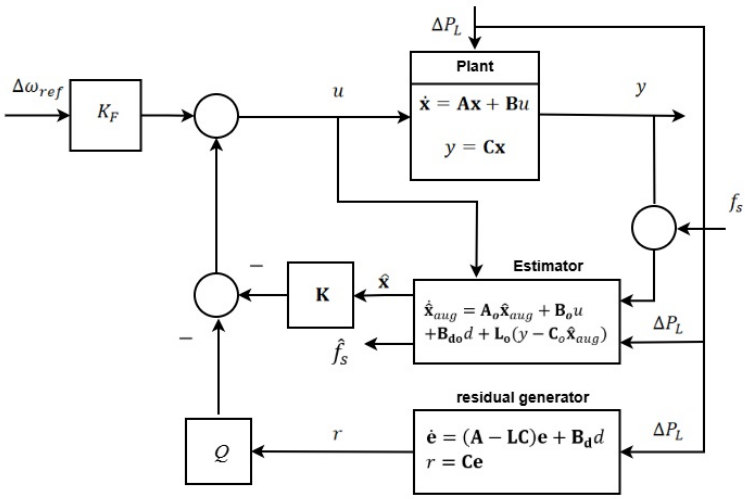


Figure 8. Schematic block diagram of the LFC system under the UCFD framework.

The derivations of three main components of the proposed UCFD framework are presented in the following sections.

4.1. Augmented State Estimator and State-Feedback Controller

To estimate and accommodate the sensor bias fault, an augmented-state estimator is employed to reconstruct the unknown sensor offset. By incorporating the sensor bias f_s into the estimator model as an additional state, the fault is transformed from an unmodeled measurement signal into an endogenous state variable. Accordingly, the augmented estimator can asymptotically reconstruct both the original system state $\mathbf{x}$ and the sensor bias f_s. As the estimation errors converge to zero, the effect of the sensor bias on the reconstructed system states is correspondingly removed, while the estimated value of f_s provides an explicit indication of the sensor fault magnitude.

Since the sensor offset f_s is assumed to be persistent or slowly varying over the time scale of the system dynamics, it can be modeled as a constant state, such that $\dot{f}_s = 0$. Accordingly, the augmented-state estimator for the LFC system in (7) and (8) is formulated as follows [37]:

$$\begin{bmatrix} \dot{\hat{\mathbf{x}}} \\ \dot{\hat{f}}_s \end{bmatrix} = \overbrace{\begin{bmatrix} \mathbf{A} & 0 \\ 0 & 0 \end{bmatrix}}^{\mathbf{A_o}} \overbrace{\begin{bmatrix} \hat{\mathbf{x}} \\ \hat{f}_s \end{bmatrix}}^{\hat{\mathbf{x}}_{aug}} + \overbrace{\begin{bmatrix} \mathbf{B} \\ 0 \end{bmatrix}}^{\mathbf{B_o}} u + \overbrace{\begin{bmatrix} \mathbf{B_d} \\ 0 \end{bmatrix}}^{\mathbf{B_{do}}} d + \mathbf{L_o}(y - \overbrace{\begin{bmatrix} \mathbf{C} & 1 \end{bmatrix}}^{\mathbf{C_o}} \begin{bmatrix} \hat{\mathbf{x}} \\ \hat{f}_s \end{bmatrix}) \tag{23}$$

where, in the context of the LFC system,

$$\mathbf{A_o} = \begin{bmatrix} -\frac{1}{\tau_g} & 0 & -\frac{1}{R\tau_g} & 0 \\ \frac{1}{\tau_T} & -\frac{1}{\tau_T} & 0 & 0 \\ 0 & \frac{1}{2H} & -\frac{D}{2H} & 0 \\ 0 & 0 & 0 & 0 \end{bmatrix}, \mathbf{B_o} = \begin{bmatrix} \frac{1}{\tau_g} \\ 0 \\ 0 \\ 0 \end{bmatrix}, \mathbf{B_{do}} = \begin{bmatrix} 0 \\ 0 \\ -\frac{1}{2H} \\ 0 \end{bmatrix},$$

$$\mathbf{C_o} = \begin{bmatrix} 0 & 0 & 1 & 1 \end{bmatrix} \text{ and } \hat{\mathbf{x}}_{aug} = \begin{bmatrix} \Delta\hat{P}_V \\ \Delta\hat{P}_m \\ \Delta\hat{\omega} \\ \hat{f}_s \end{bmatrix} \tag{24}$$

Consequently, the augmented state estimator is implemented as

$$\dot{\hat{\mathbf{x}}}_{aug} = (\mathbf{A_o} - \mathbf{L_o}\mathbf{C_o})\hat{\mathbf{x}}_{aug} + \mathbf{B_o}u + \mathbf{B_{do}}d + \mathbf{L_o}y \tag{25}$$

where u, $d = \Delta P_L$, and y denote the control input, load disturbance, and measured output, respectively, while $\hat{\mathbf{x}}_{\text{aug}}$ denotes the augmented state estimate and $\mathbf{L_o}$ is the augmented estimator gain.

The design of the state-feedback controller $\mathbf{K}$, based on the estimated system state vector $\hat{\mathbf{x}}$, follows the same procedure presented in Section 3.2, prior to the augmentation of the integral state x_I. Specifically, the controller gain $\mathbf{K}$ and the augmented estimator gain $\mathbf{L}_o$ are determined using the pole-placement technique. The closed-loop poles are selected such that the eigenvalues of $(\mathbf{A} - \mathbf{BK})$ and $(\mathbf{A_o} - \mathbf{L_o}\mathbf{C_o})$ provide the desired control and estimation dynamics, respectively.

4.2. Reference Tracking Using a FeedForward Controller K_F

To overcome the undesirable behavior associated with integral action, which accumulates measurement errors in the presence of sensor bias fault while maintaining reference tracking capability, a feedforward controller is adopted. Accordingly, prior to incorporating the residual generator component discussed in the next section, the control law is expressed as

$$u = K_F r_{ref} - \mathbf{K}\hat{\mathbf{x}} \tag{26}$$

To ensure zero steady-state error for a constant reference signal, the steady-state values of the state variables and control input corresponding to zero output error ($y = r_{ref}$) are first determined, after which the control law is designed to regulate the system toward these equilibrium conditions [35].

Following the state-space reference scaling approach presented in [35], the feedforward gain K_F is obtained as

$$K_F = N_u + \mathbf{K}\mathbf{N}_x \tag{27}$$

where $\mathbf{K}$ denotes the state-feedback gain, while N_u and $\mathbf{N}_x$ are computed from

$$\begin{bmatrix} \mathbf{N_x} \\ N_u \end{bmatrix} = \begin{bmatrix} \mathbf{A} & \mathbf{B} \\ \mathbf{C} & 0 \end{bmatrix}^{-1} \begin{bmatrix} \mathbf{0} \\ 1 \end{bmatrix} \tag{28}$$

However, in the context of LFC, N_u and $\mathbf{N}_x$ are obtained by substituting $\mathbf{A}, \mathbf{B}$, and $\mathbf{C}$ of (9) and (10) in (28) as

$$\begin{bmatrix} \mathbf{N_x} \\ N_u \end{bmatrix} = \begin{bmatrix} -\frac{1}{\tau_g} & 0 & -\frac{1}{R\tau_g} & \frac{1}{\tau_g} \\ \frac{1}{\tau_T} & -\frac{1}{\tau_T} & 0 & 0 \\ 0 & \frac{1}{2H} & -\frac{D}{2H} & 0 \\ 0 & 0 & 1 & 0 \end{bmatrix}^{-1} \begin{bmatrix} 0 \\ 0 \\ 0 \\ 1 \end{bmatrix} \tag{29}$$

4.3. Residual Generator and Auxiliary Feedback Controller $Q(s)$

The residual generator and the auxiliary feedback controller $Q(s)$ constitute the disturbance-rejection component of the proposed UCFD framework, whose primary function is to mitigate the effect of load disturbances on the system frequency. In particular, an additional load demand introduces a discrepancy between the actual system response and its corresponding estimated response. This discrepancy is represented by the residual signal $r(t)$, defined as

$$r(t) = y(t) - \hat{y}(t), \tag{30}$$

where $y(t)$ and $\hat{y}(t)$ denote the measured and estimated system outputs, respectively. Accordingly, the residual signal can be characterized as

$$r(t) = \begin{cases} 0, & \text{under no-demand disturbance conditions,} \\ \neq 0, & \text{in the presence of a load disturbance.} \end{cases}$$

Thus, a nonzero residual provides an indication of the discrepancy introduced by an additional load demand and is subsequently utilized by the auxiliary feedback controller $Q(s)$. The resulting compensation signal is incorporated into the control action to counteract the adverse effect of the load disturbance on the system frequency response. In this manner, the residual-driven feedback path provides an additional disturbance-rejection mechanism without relying on the accumulation of tracking errors inherent to integral control concept.

The dynamics of the residual signal $r(t)$ are governed by the state-estimation error ($\mathbf{e} = \mathbf{x} - \hat{\mathbf{x}}$), which, in the present formulation caused by the load disturbance ($d = \Delta P_L$). To characterize the residual generation mechanism, consider the LFC system described by

$$\dot{\mathbf{x}} = \mathbf{A}\mathbf{x} + \mathbf{B}u + \mathbf{B_d}d \tag{31}$$

$$y = \mathbf{C}\mathbf{x} \tag{32}$$

together with a state estimator

$$\dot{\hat{\mathbf{x}}} = \mathbf{A}\hat{\mathbf{x}} + \mathbf{B}u + \mathbf{L}(y - \hat{y}) \tag{33}$$

hence the residual dynamics can consequently be expressed as [30,37]

$$\dot{\mathbf{e}} = (\mathbf{A} - \mathbf{LC})\mathbf{e} + \mathbf{B_d}d \tag{34}$$

$$r = y - \hat{y} = \mathbf{Ce} \tag{35}$$

where the residual signal (r) is driven by the load demand d only. The estimator gain $\mathbf{L}$ is selected to ensure sufficiently fast and stable convergence of the state-estimation error. In particular, the eigenvalues of the estimator error dynamics matrix $(\mathbf{A} - \mathbf{LC})$ are assigned using the pole-placement technique.

Accordingly, the residual-driven compensation signal generated through $Q(s)$ is incorporated into the control input to counteract the adverse effect of load disturbances on the frequency response. In this way, the disturbance-rejection mechanism operates independently of the sensor-bias estimation mechanism described in the preceding section. Specifically, the sensor bias (f_s) is reconstructed by the augmented-state estimator and its effect is removed through the use of the corrected state estimate, whereas the residual generator and $Q(s)$ are retained primarily to compensate for the effect of load-demand variations. This separation of functions is a key feature of the proposed UCFD architecture, as it enables sensor-fault accommodation and disturbance rejection to be addressed through distinct and explicitly defined mechanisms. Thus, the full control law of UCFD would be expressed as

$$u = K_F r_{ref} - \mathbf{K}\hat{\mathbf{x}} - Qr \tag{36}$$

As the state-feedback controller and feedforward compensator are responsible for stabilization and reference tracking, respectively, the auxiliary feedback controller is required to reject the effects of constant or slowly varying disturbances on the frequency deviation $(\Delta\omega)$. Accordingly, a first-order auxiliary compensator structure is considered as

$$Q(s) = \frac{K_Q}{\tau_Q s + 1} \in RH_\infty, \tag{37}$$

where K_Q and τ_Q denote the compensator gain and time constant, respectively. An analytical value for K_Q is obtained in the following proposition, while a suggested value for τ_Q is given in the subsequent remark.

Proposition 1. *Consider the closed-loop system subject to a constant load demand $d = \Delta P_L$. With an auxiliary feedback controller $Q(s)$ driven by the residual signal $r(t)$, then the steady-state frequency deviation satisfies*

$$\Delta\omega_{ss} = 0$$

provided that the compensator gain is selected as

$$K_Q = -\frac{\mathbf{C}(\mathbf{A} - \mathbf{BK})^{-1}\mathbf{B_d}}{[\mathbf{C}(\mathbf{A} - \mathbf{BK})^{-1}\mathbf{B}] \cdot [\mathbf{C}(\mathbf{A} - \mathbf{LC})^{-1}\mathbf{B_d}]} \tag{38}$$

Proof. The proof follows from the steady-state residual dynamics and the fault-accommodation condition $y_{ss} = 0$. A complete derivation is provided in Appendix A. □

Remark 1. *The compensator time constant (τ_Q) is selected according to*

$$\tau_Q = \frac{\alpha}{\min|\Re(\lambda(\mathbf{A} - \mathbf{LC}))|} \qquad \alpha \geq 5, \tag{39}$$

where $\Re(\lambda(\mathbf{A} - \mathbf{LC}))$ denote the real part of the observer poles. The parameter α is chosen such that τ_Q exceeds at least five dominant observer time constants. That choice ensures that the residual signal r is primarily dominated by disturbances before compensation action is generated. As a result, a clear time-scale separation is established between the observer and the auxiliary compensator dynamics (see, Appendix B).

The gain K_Q given by (38) and the time constant τ_Q given by (39) are to be used as an initial value and can subsequently be refined to achieve the desired transient performance.

4.4. Simulation Case Study 2

The isolated power station considered in Section 3.3 is reconsidered under the same operating scenarios, with the proposed UCFD framework applied to evaluate its performance. For consistency and comparison purposes, the estimator and state-feedback controller are designed with comparable dynamic characteristics by appropriately selecting their respective closed-loop poles.

First, the augmented-estimator gain ($\mathbf{L_o}$) is determined using the `place` command in MATLAB, which implements the pole-placement technique. The observer poles are assigned as

$$-29.43, \quad -2.984 \pm 2.88i, \quad -3.$$

The additional observer pole at -3 is introduced to govern the dynamics associated with the augmented sensor-bias state. Accordingly, using the matrices ($\mathbf{A_o}^T$) and ($\mathbf{C_o}^T$) defined in (24), the resulting augmented-estimator gain is obtained as

$$\mathbf{L_o} = 10^2 \times \begin{bmatrix} 19.637 \\ 6.236 \\ -0.413 \\ 0.726 \end{bmatrix}.$$

The state-feedback gain ($\mathbf{K}$) is subsequently determined using the `place` command by assigning the closed-loop poles to

$$-17.65, \quad -1.763 \pm 5.328i$$

The resulting state-feedback gain is

$$\mathbf{K} = \begin{bmatrix} 2.824 & 5.427 & 530.649 \end{bmatrix}.$$

With the state-feedback gain determined, the feedforward gain K_F in (27) is then calculated. The quantities N_u and $\mathbf{N}_x$, obtained from (28), are required for its computation. These quantities are given by

$$N_u = 20.8, \qquad \mathbf{N}_x = \begin{bmatrix} 0.8 \\ 0.8 \\ 1.0 \end{bmatrix}.$$

Consequently, the resulting feedforward gain is

$$K_F = 561.6$$

For the residual-generation mechanism, the matrices $\mathbf{A}$, $\mathbf{C}$, and $\mathbf{B_d}$ are defined according to the disturbance-driven model in (31). The residual-generator observer gain $\mathbf{L}$ is then obtained using the `place` command by assigning its poles to values corresponding to $5 \times eig(\mathbf{A})$. The resulting gain is

$$\mathbf{L} = 10^2 \times \begin{bmatrix} 100.5 \\ 5.24 \\ 0.28 \end{bmatrix}.$$

Finally, the auxiliary feedback controller Q(s) is synthesized to provide disturbance-rejection capability. The gain (K_Q) is calculated from (38), yielding

$$K_Q = 2.382 \times 10^4$$

The corresponding time constant (τ_Q) is determined from (39)

$$\tau_Q \approx 1.7$$

where $\min|\Re\lambda(\mathbf{A}-\mathbf{LC})| \approx 2.939$ and $\alpha = 5$ are considered. Accordingly, the auxiliary feedback controller $Q(s)$ is obtained as

$$Q(s) = \frac{2.382 \times 10^4}{1.7s + 1} \in RH_\infty$$

The controller is driven by the residual signal (r) and generates an auxiliary compensation signal to mitigate the adverse effects of load disturbances on the system frequency response.

With all controller and estimator gains determined, the isolated power station is simulated in the MATLAB R2018b/Simulink environment under the operating scenarios defined in Section 3.3. The resulting responses are subsequently evaluated to assess the disturbance-rejection and sensor-fault accommodation capabilities of the proposed UCFD framework.

Case 1: This case study investigates the dynamic response of the proposed UCFD-based LFC system under a step load disturbance of $\Delta P_L = 0.2$ p.u. applied at ($t = 15$ s), as illustrated in Figure 9. Figure 9a–d compare the actual state variables $\Delta P_v, \Delta P_m, \Delta\omega$, and the sensor bias f_s with their corresponding estimates, namely, $\Delta\hat{P}_v, \Delta\hat{P}_m, \Delta\hat{\omega}$, and $\hat{f}_s$, respectively. Figure 9e presents the resulting residual signal $r(t)$.

Prior to the application of the load disturbance ($t < 15$ s), the augmented estimator provides accurate and unbiased reconstruction of all system states, while the estimated sensor bias remains at zero. Moreover, the residual signal remains zero, i.e., ($r = 0$), confirming that the system operates under nominal conditions without an active disturbance or sensor-bias fault. The close agreement between the actual and estimated outputs further demonstrates the satisfactory estimation performance of the proposed augmented observer.

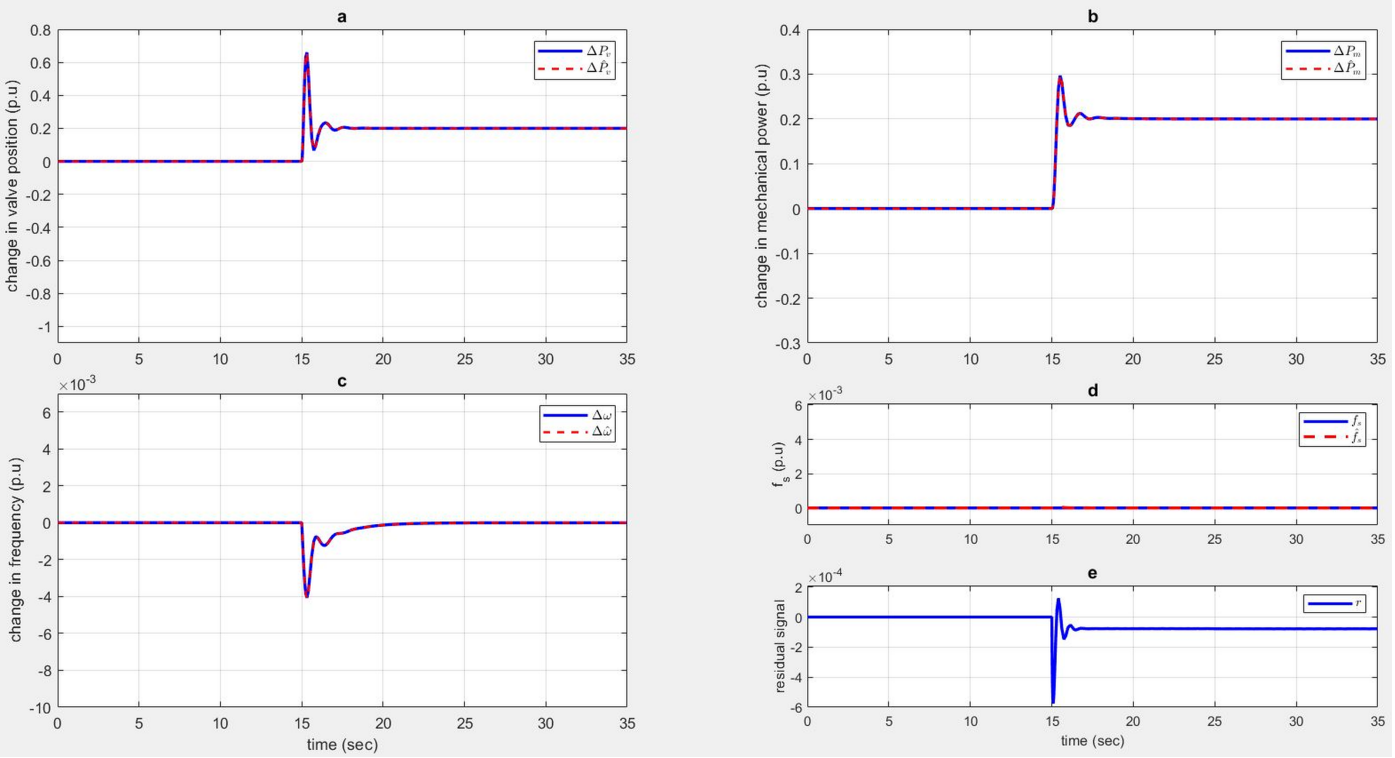


Figure 9. Response of the LFC system under the UCFD framework for $\Delta P_L = 0.2$ p.u. at 15 s: (**a**) change in valve position, (**b**) change in mechanical power, (**c**) change in frequency, (**d**) sensor bias fault, and (**e**) residual signal.

At ($t = 15$ s), the step load disturbance of $\Delta P_L = 0.2$ p.u. is applied to the system. As shown in Figure 9a–d, the actual and estimated state trajectories remain closely matched throughout the disturbance response, with the estimates exhibiting negligible steady-state bias. In particular, the estimated sensor bias remains at zero, indicating that the load disturbance is correctly distinguished from a sensor-bias fault. This behavior is attributed to the explicit incorporation of the load disturbance into the augmented observer model, which enables the estimator to account for its effect while reconstructing the system state variables.

Although the load disturbance is accommodated within the state-estimation process, it simultaneously excites the residual-generation mechanism, producing a nonzero residual signal ($r \neq 0$), as shown in Figure 9e. The generated residual therefore provides an indication of the load-disturbance condition and is subsequently supplied to the auxiliary feedback controller $Q(s)$. The resulting compensation signal counteracts the adverse effect of the load disturbance and contributes to restoring the system frequency to its nominal value.

As a result, the proposed UCFD framework maintains a well-damped transient response with negligible oscillatory behavior and achieves complete elimination of the steady-state frequency error. Compared with the integral-control approach considered previously, however, the proposed UCFD framework exhibits a somewhat slower transient response, with a settling time of approximately 6 s.

Case 2: This case study investigates the performance of the proposed UCFD-based LFC framework under simultaneous load-disturbance and sensor-bias fault conditions. A step load disturbance of $\Delta P_L = 0.2$ p.u. is applied at $t = 15$ s, followed by the introduction of a sensor-bias fault of magnitude $f_s = 0.005$ p.u. at $t = 25$ s. These operating conditions correspond to those considered previously in Case 2 of the integral-control approach, thereby providing a direct basis for comparison. The resulting system responses are presented in Figure 10.

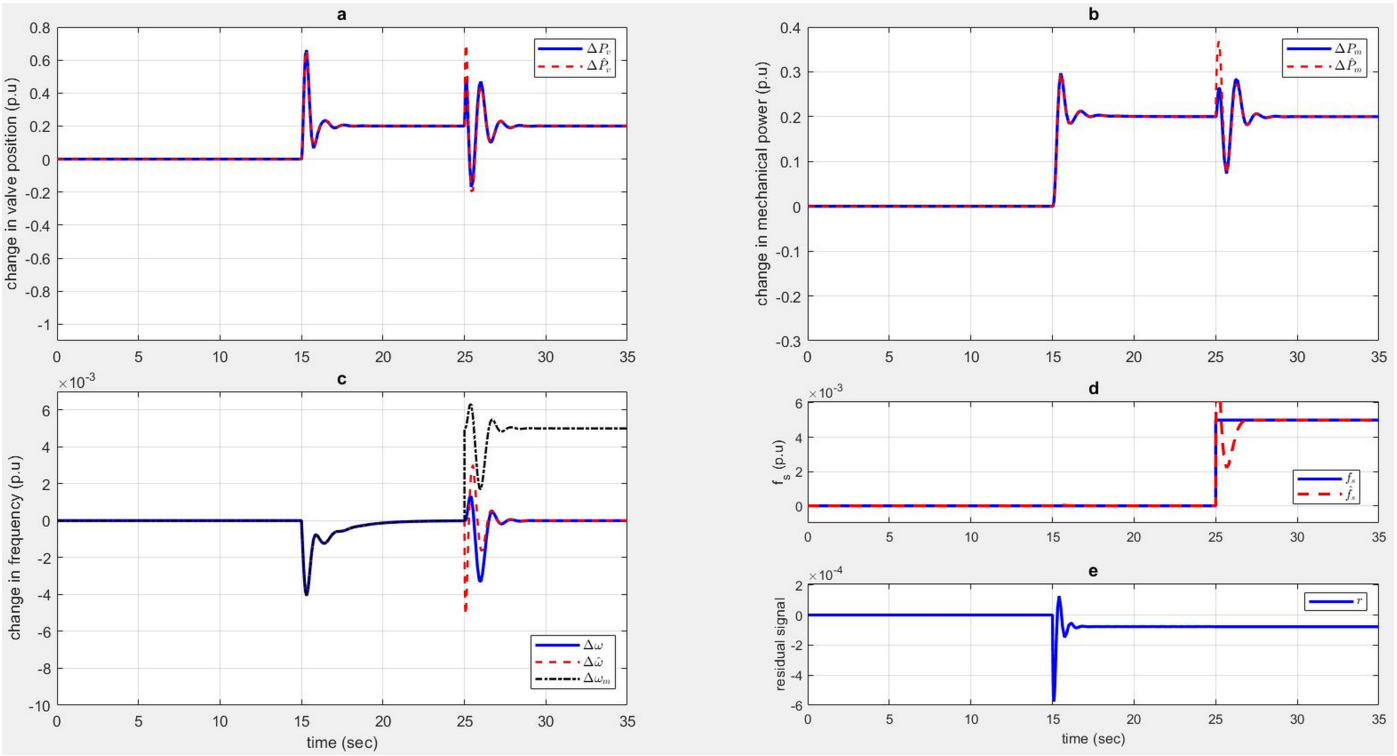


Figure 10. Response of the LFC system under the UCFD framework for $\Delta P_L = 0.2$ p.u. at 15 s with sensor bias fault of $f_s = 0.005$ p.u. for $t \geq 25$ s: (**a**) change in valve position, (**b**) change in mechanical power, (**c**) change in frequency, (**d**) sensor bias fault, and (**e**) residual signal.

As shown in Figure 10a–d, the proposed augmented estimator accurately reconstructs the system states throughout both the load-disturbance and sensor-fault conditions. Following the application of the load disturbance at $t = 15$ s, the estimated state trajectories closely follow their actual counterparts, with negligible steady-state estimation error. More importantly, following the sensor-bias fault at $t = 25$ s, no persistent bias is introduced into the estimated states $\Delta\hat{P}_v$, $\Delta\hat{P}_m$, and $\Delta\hat{\omega}$. This behavior results from explicitly augmenting the sensor bias f_s as an additional state in the estimator. Thus, the augmented observer dynamically reconstructs the sensor bias and separates its contribution from the actual system states.

The distinction between the actual frequency deviation and its corrupted measurement is particularly evident in Figure 10c. Before the occurrence of the sensor fault, the measured frequency deviation $\Delta\omega_m$ and the actual frequency deviation $\Delta\omega$ coincide. At $t = 25$ s, however, the sensor bias causes the measured frequency to exhibit an abrupt offset, such that

$$\Delta\omega_m = \Delta\omega + f_s,$$

and consequently $\Delta\omega_m$ changes by approximately 0.005 p.u. Although the measured signal is therefore corrupted, the actual frequency deviation $\Delta\omega$ remains effectively regulated around its nominal value. Simultaneously, the augmented estimator reconstructs the clean frequency deviation $\Delta\hat{\omega}$ and provides an estimate of the sensor bias $\hat{f}_s$, as illustrated in Figure 10c,d, respectively. Hence, the sensor fault is not interpreted as a genuine frequency deviation by the state-feedback controller.

The effectiveness of this separation is further supported by the residual response shown in Figure 10e. Immediately after the load disturbance at $t = 15$ s, the residual generator produces a pronounced nonzero residual ($r \neq 0$), indicating the presence of a load-disturbance condition. The residual is consequently supplied to the auxiliary feedback controller (Q(s)), which generates the required compensation to counteract the effect of the load disturbance. In contrast, the subsequent sensor-bias fault at $t = 25$ s does not produce a comparable disturbance residual. This behavior demonstrates that the proposed architecture separates the two effects: the load disturbance is addressed through the residual-driven compensation path, whereas the sensor bias is accommodated through the augmented state estimator. Accordingly, the two control mechanisms operate using appropriately reconstructed information. The state-feedback controller acts on the estimated system states, which remain effectively free from the sensor bias fault after the augmented estimator reconstructs f_s. At the same time, the auxiliary controller $Q(s)$ is driven by the residual associated with the load disturbance rather than by the corrupted frequency measurement. Consequently, neither control path is misled by the sensor offset, and the frequency-regulation mechanism continues to respond to the actual system condition rather than to the biased measurement.

As a result, the frequency deviation $\Delta\omega$ exhibits a well-damped transient response with negligible oscillatory behavior and converges to zero in steady-state despite the simultaneous presence of a load disturbance and a biased frequency measurement. This result highlights a fundamental advantage of the proposed UCFD framework over the integral-control approach. In the latter, the integral action operates directly on the biased tracking error and therefore accumulates the sensor offset, causing the controller to regulate the corrupted measurement rather than the actual frequency, see Figure 5a,c and Figure 6a, respectively. In contrast, the proposed framework explicitly reconstructs the sensor bias and separates it from the physical system states. Thus, the state-feedback controller continues to regulate the actual frequency dynamics, while the residual-driven $Q(s)$ compensates for the load disturbance, providing effective disturbance rejection together with enhanced resilience to sensor bias faults.

Case 3: This case study investigates the scenario in which the sensor bias fault occurs prior to the load disturbance. Specifically, the sensor fault is introduced at $t \geq 5$ s, followed

by a load demand at $t \geq 15$ s. As shown previously for the integral control approach in Figure 6a, the frequency response becomes unsatisfactory due to the offset measurement misleading the integral action from an early stage. In contrast, the proposed UCFD framework successfully maintains satisfactory frequency regulation performance, shown in Figure 11a. Consequently, the adverse effects of the sensor bias fault and the subsequent disturbance are effectively compensated, resulting in a well-damped $\Delta\omega$ response with negligible steady-state error. Moreover, Figure 11b illustrates the dynamic response of the control signal $u(t)$ under the considered operating conditions. At $t = 5$ s, the sudden introduction of the positive sensor-bias fault f_s induces an immediate transient spike in the control signal. Unlike the integral-control response, which exhibits a pronounced and abrupt change in the control action following the sensor bias, the proposed UCFD framework limits this effect to a transient response and subsequently restores the control signal to its nominal zero baseline. Following the application of the load disturbance $\Delta P_L = 0.2$ p.u. at $t = 15$ s, the control signal exhibits a characteristic positive transient effort and subsequently converges to a steady-state value of approximately 0.2 p.u., thereby providing the required generation adjustment to restore the power balance and maintain the system frequency at its nominal value.

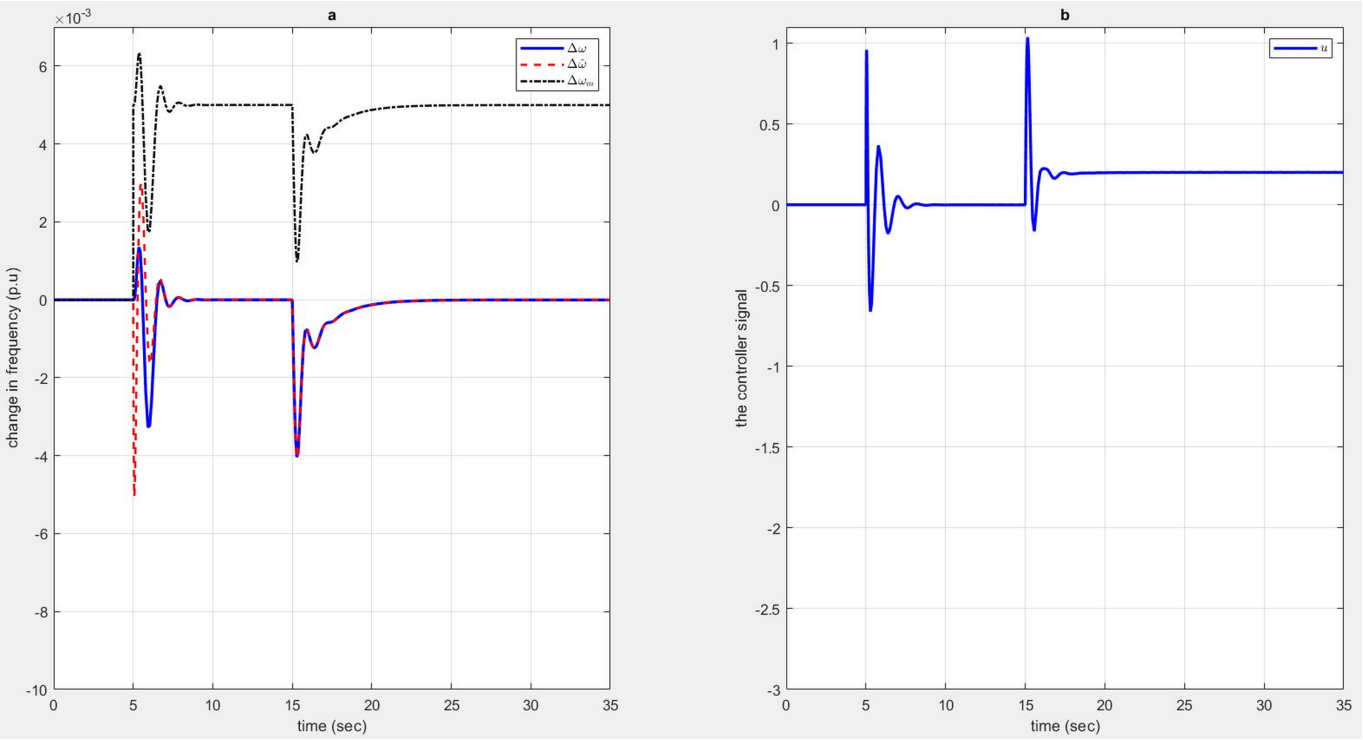


Figure 11. Response of the LFC system under the UCFD framework for $\Delta P_L = 0.2$ p.u. at 15 s with sensor bias fault of $f_s = 0.005$ p.u. for $t \geq 5$ s: (**a**) change in frequency and (**b**) the controller signal.

Case 4: This case study aims to evaluate the resilience of the proposed UCFD framework under the same realistic operating conditions, the identical parameter uncertainties, stochastic load fluctuations, and persistent sensor bias fault considered in Case 4 of Section 3.3 are applied without modification.

The resulting responses are presented in Figure 12. As shown in Figure 12a, the sensor bias fault introduced at $t = 5$ s causes the measured frequency $\Delta\omega_m$ to shift toward approximately 0.005 p.u., as expected from the imposed measurement bias. In contrast, the actual frequency deviation $\Delta\omega$ remains centered around zero after the initial transient, while the estimated frequency $\Delta\hat{\omega}$ closely tracks the physical frequency response. Compared with the nominal condition response, however, the convergence of $\Delta\hat{\omega}$ toward $\Delta\omega$ is noticeably

slower under the imposed parameter uncertainty. Nevertheless, the estimated frequency ultimately converges to the actual frequency despite the simultaneous parameter mismatch and stochastic load fluctuations.

The load step applied at $t = 15$ s produces a second transient in both the actual and estimated frequency responses. Following this disturbance, $\Delta\omega$ and $\Delta\hat{\omega}$ return toward zero, while the remaining small fluctuations around the zero operating point are associated primarily with the stochastic component of the load disturbance. Importantly, the persistent sensor bias does not produce a corresponding steady-state bias in the physical frequency. This demonstrates that the augmented-state observer can reconstruct the sensor bias component despite the presence of parameter uncertainty, thereby preventing the state-feedback controller from interpreting the measurement error as a genuine frequency deviation.

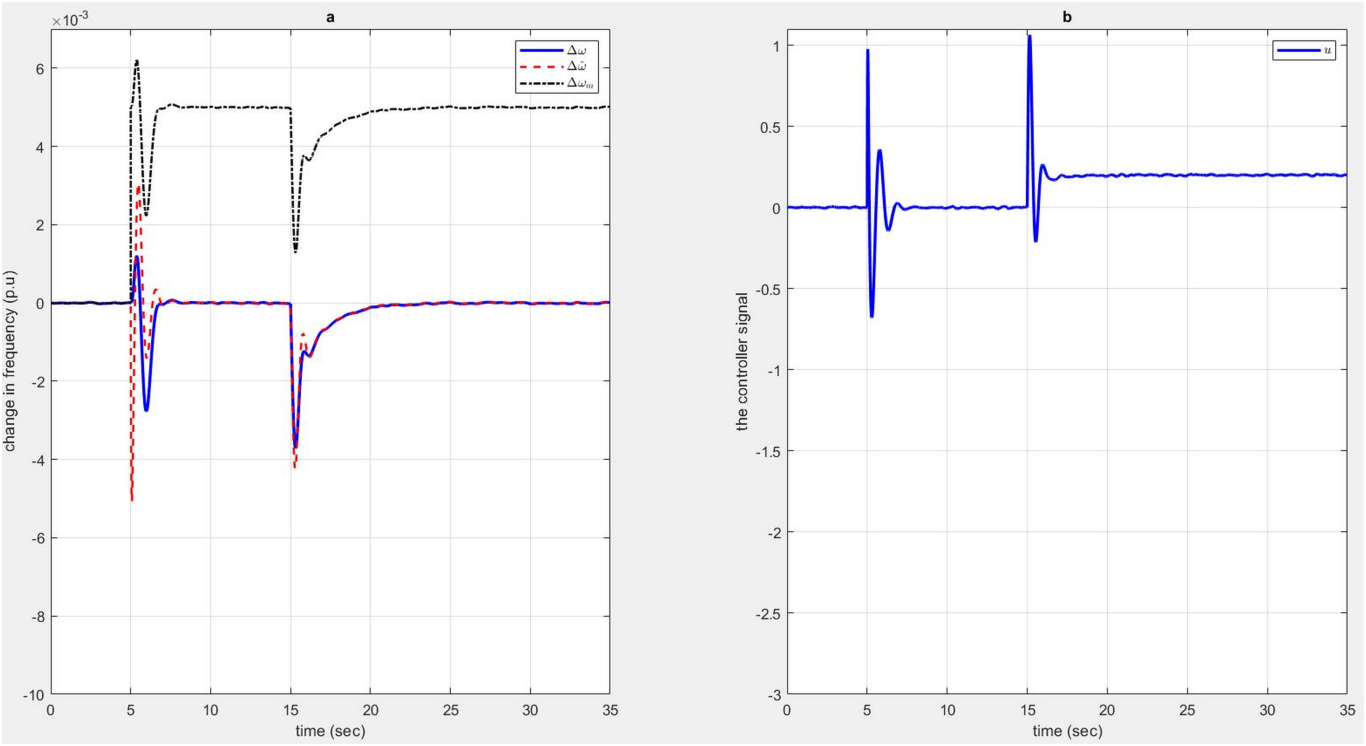


Figure 12. Response of the LFC system under the proposed UCFD framework for $\Delta P_{L,\text{step}} = 0.2$ p.u. at 15 s and a sensor-bias fault of $f_s = 0.005$ p.u. for $t \geq 5$ s: (**a**) change in frequency and (**b**) the controller signal.

Figure 12b illustrates the corresponding control signal $u(t)$. The sensor bias fault at $t = 5$ s produces a negative transient of approximately -0.7 p.u., which is substantially smaller than the approximately -2.7 p.u. transient observed with the integral control approach in Figure 7b. This reduction indicates that reconstructing the sensor bias at the estimation level prevents the persistent measurement error from generating an excessive corrective control action. The load step at $t = 15$ s produces another pronounced transient, whose magnitude is comparable to, and slightly larger than, that observed under integral control. Thus, the advantage of the UCFD framework should not be interpreted as a uniform reduction in the peak control amplitude; rather, its principal benefit is the avoidance of the excessive fault-induced control transient and the associated erroneous steady-state control bias.

Following the transients, the UCFD control signal settles around approximately 0.2 p.u., which is consistent with the applied physical load step. In contrast, the integral controller settles around a lower biased level because part of its control action is devoted to compensating for the persistent sensor error. The UCFD control signal also exhibits stochastic fluctuations due to the random load component.

Overall, Case 4 demonstrates that the proposed UCFD framework maintains near-zero physical frequency deviation in the presence of simultaneous parameter uncertainty, stochastic load variations, and a persistent sensor bias fault. Although the parameter mismatch results in slower state-estimation convergence, the augmented observer ultimately reconstructs the physical frequency without a persistent bias. Moreover, by accommodating the sensor fault at the estimation level, the proposed framework avoids the excessive fault-induced control transient and the erroneous steady-state control offset observed with integral action. These results demonstrate the ability of the proposed architecture to preserve frequency regulation under combined modeling uncertainty, stochastic disturbances, and sensor faults.

Finally, while the simulations presented in this study utilize a baseline sensor bias magnitude of $f_s = 0.005$ p.u. to clearly illustrate the fundamental vulnerability of integral control and the effectiveness of the proposed UCFD framework, the underlying observer-based architecture is linear with respect to the fault magnitude. Consequently, the framework's ability to asymptotically reconstruct and accommodate the sensor bias scales proportionally for both lower and upper values of the fault size. For lower bias magnitudes, representing minor sensor calibration drifts or early-stage degradation, the augmented-state observer will reconstruct a correspondingly smaller $\hat{f}_s$, allowing the state-feedback controller to seamlessly compensate for the subtle measurement offset. Conversely, for upper bias magnitudes, representing more severe sensor anomalies, the observer will reconstruct a proportionally larger $\hat{f}_s$, and the state-feedback controller will continue to operate effectively on the unbiased state estimates. Because the fault accommodation is handled entirely at the estimation level rather than through integral error accumulation, the proposed UCFD framework maintains its structural integrity and robustness regardless of the fault severity, ensuring reliable frequency regulation across a wide range of sensor anomalies in practical LFC applications.

5. Quantitative Evaluation

To quantitatively evaluate the frequency regulation performance of both the integral control approach and the proposed UCFD framework under the considered operating scenarios, the integral squared error (ISE) criterion is employed. The performance index is defined based on the tracking error signal

$$e(t) = y(t) - r_{ref}(t) \tag{40}$$

where the corresponding ISE is calculated as [38]

$$J = \int_0^{t_{end}} e^2(\tau)\, d\tau. \tag{41}$$

In the present work, the system output corresponds to the frequency deviation $y(t) = \Delta\omega(t)$, while the reference signal is selected as the nominal operating condition $r_{ref}(t) = \Delta\omega_{ref} = 0$. Accordingly, the performance index reduces to

$$J = \int_0^{35\ sec} \Delta\omega^2(\tau)\, d\tau. \tag{42}$$

The obtained ISE values for the investigated cases are summarized in Table 2.

The obtained values of J demonstrate the superior overall performance of the proposed UCFD framework compared with the integral control approach in Cases: 2, 3, and 4. Specifically, in Case 2, the UCFD framework reduces the ISE from 2.6007×10^{-4} to 1.2821×10^{-5}. In Case 3, the improvement is even more pronounced, lowering the cumulative squared error from 7.7432×10^{-4} to 1.2808×10^{-5}. Furthermore, in Case 4, the framework reduces the ISE from 7.7523×10^{-4} to 1.0959×10^{-5}. These significantly lower ISE values indicate improved frequency regulation and disturbance rejection performance over the considered simulation interval, particularly under load disturbance and sensor bias fault conditions.

These results are consistent with the observed transient responses, which exhibit improved damping and effective elimination of the steady-state frequency error despite the presence of biased measurements. Nevertheless, under normal operating conditions without sensor faults, the integral control approach achieves a lower ISE than the proposed UCFD framework, indicating slightly better nominal tracking performance in the absence of abnormal operating conditions. This trade-off reflects the principal advantage of the proposed framework: while the integral control approach may provide marginally better nominal performance, the UCFD framework offers substantially greater robustness to load disturbances and sensor bias faults.

Table 2. ISE comparison between the integral control approach of Case Study 1 and the proposed UCFD framework of Case Study 2.

Case	Integral Control Approach	UCFD Framework
Case 1	5.6475×10^{-6}	7.7394×10^{-6}
Case 2	2.6007×10^{-4}	1.2821×10^{-5}
Case 3	7.7432×10^{-4}	1.2808×10^{-5}
Case 4	7.7523×10^{-4}	1.0959×10^{-5}

To assess the actuator demands associated with the two control strategies, the control input $u(t)$ is evaluated using two complementary metrics. While the integral of squared error (ISE) of the frequency deviation quantifies the overall frequency-regulation performance, the control effort is characterized by the integral squared control effort (ISCE), denoted by J_{u^2}, and the maximum absolute control input, $u_{\max}$. These metrics are defined as

$$J_{u^2} = \int_0^{t_{\text{end}}} u^2(\tau)\, d\tau, \tag{43}$$

which quantifies the cumulative squared magnitude of the control input over the simulation interval, and

$$u_{\max} = \max_{0 \le t \le t_{\text{end}}} |u(t)|, \tag{44}$$

which characterizes the maximum instantaneous control demand and provides an indication of the potential for actuator saturation and excessive peak loading. The resulting values of J_{u^2} and $u_{\max}$ for the investigated scenarios, including nominal, faulty, and uncertain operating conditions, are summarized in Table 3.

Table 3. Control-effort metrics for the integral control approach and the UCFD framework.

Case	Integral Control Approach		UCFD Framework	
	J_{u^2}	$u_{\max}$	J_{u^2}	$u_{\max}$
Case 1	1.002	0.970	0.970	1.036
Case 2	1.546	2.530	1.161	1.174
Case 3	1.339	2.730	1.172	1.036
Case 4	1.244	2.730	1.175	1.063

As shown in Table 3, under nominal operating conditions (Case 1), the two control strategies exhibit comparable cumulative squared control effort. The UCFD framework yields a slightly lower J_{u^2}, decreasing from 1.002 to 0.970, although this is accompanied by a small increase in the peak control input from 0.970 to 1.036. Thus, under nominal conditions, the proposed framework does not provide a uniform reduction in both control-effort metrics.

A more pronounced difference is observed under faulty and uncertain operating conditions. In Case 2, the UCFD framework reduces J_{u^2} from 1.546 to 1.161 and decreases

$u_{\max}$ from 2.530 to 1.174. Similarly, in Case 3, J_{u^2} is reduced from 1.339 to 1.172, while the peak control input decreases substantially from 2.730 to 1.036. In Case 4, which incorporates parameter uncertainty, stochastic load fluctuations, and a persistent sensor-bias fault, the UCFD framework also achieves a lower cumulative squared control effort, with J_{u^2} decreasing from 1.244 to 1.175, while $u_{\max}$ is reduced from 2.730 to 1.063.

These results indicate that, under faulty and stressed operating conditions, the UCFD framework not only reduces the magnitude of the largest control excursions but also requires a lower cumulative squared control effort. The substantial reduction in $u_{\max}$ is particularly relevant because large transient control commands can increase the likelihood of actuator saturation and impose excessive instantaneous loading. The simultaneous reduction in J_{u^2} further indicates that the proposed framework does not achieve this reduction in peak demand merely by generating larger control actions elsewhere in the response.

This behavior can be attributed to the separation of sensor fault accommodation and load-disturbance rejection within the proposed architecture. The augmented-state observer reconstructs the sensor bias fault and provides corrected state estimates for feedback control, thereby preventing the persistent measurement error from being interpreted as an actual frequency deviation. Meanwhile, the residual-generation observer and the auxiliary compensator $Q(s)$ provide a dedicated path for load-disturbance rejection. Consequently, the feedback controller is less prone to generating excessive corrective action in response to sensor-induced measurement errors.

Overall, the results demonstrate that the proposed UCFD framework provides a favorable control-effort profile under the considered faulty and uncertain operating conditions. In particular, the simultaneous reduction in cumulative squared control effort and peak control demand in Cases 2–4 indicates that the improved frequency-regulation performance is not obtained at the expense of increased actuator demand. Although a small increase in peak control input is observed under nominal conditions, the pronounced reductions in both J_{u^2} and $u_{\max}$ under faulty conditions highlight the actuator-demand benefits of accommodating sensor faults at the estimation level.

6. Conclusions and Future Directions

This article presented a unified control and fault diagnosis (UCFD) framework for single-area load frequency control (LFC) systems subject to load disturbances and sensor-bias faults. The proposed framework replaces conventional integral action with a state-feedback and feedforward control structure and employs two dedicated observers with complementary functions. The augmented-state observer incorporates the operationally available load-demand variation ΔP_L and reconstructs both the system states and the sensor bias fault f_s, while the second observer generates a residual associated with load disturbances for the auxiliary first-order compensator Q. This separation allows sensor bias accommodation to be performed at the estimation level while load-disturbance rejection is achieved through the residual-driven compensation path.

The simulation results demonstrate that the proposed framework maintains accurate state reconstruction and negligible steady-state frequency deviation in the presence of sensor bias, thereby avoiding the fundamental vulnerability of integral control to persistent measurement errors. In contrast, the integral control may force the corrupted measured frequency toward zero while leaving the actual frequency biased. Although integral control provides better performance in the fault-free load-disturbance case, the proposed UCFD framework achieves improved frequency regulation performance under the faulty and disturbed operating conditions considered, as demonstrated by the J, J_{u^2}, and u_{max} evaluations. Overall, the results confirm the effectiveness of separating state estimation, sensor bias fault accommodation, and load-disturbance rejection within a unified control architecture.

Although the present study demonstrates resilience to persistent sensor biases, parameter uncertainties, and stochastic load variations, practical power systems may also experience intermittent measurement distortions caused by phenomena such as poor wiring contacts or electromagnetic interference (EMI). The rapid and transient nature of such faults may require observer designs with enhanced tracking capabilities, including high-gain or sliding-mode observer variants. Future work will therefore investigate the development and evaluation of detection criteria and accommodation strategies for intermittent sensor faults, together with practical nonlinearities such as governor deadband (GDB) and generation rate constraints (GRCs), which may introduce additional plant–model mismatch and affect estimation and transient frequency-regulation performance.

Further extensions will consider interconnected multi-area LFC systems and additional fault scenarios, including governor-valve and actuator faults. In multi-area systems, the increased number of generation states and tie-line dynamics introduces additional scalability and coupling challenges, while disturbances and faults in one area may influence neighboring areas and complicate residual interpretation and fault localization. These challenges motivate the development of decentralized or distributed UCFD architectures that explicitly account for inter-area coupling while exploiting the sparse structure of interconnected power systems.

Finally, beyond the investigated AC load frequency control application, the proposed UCFD framework offers a potential methodological foundation for developing resilient and fault-tolerant control strategies in DC energy distribution systems. In particular, the separation of sensor-bias estimation and load-disturbance rejection, achieved through the augmented-state observer and residual-based auxiliary compensator, could be adapted to DC-bus voltage regulation, where sensor inaccuracies and constant-power load fluctuations may compromise voltage stability and control performance.

Author Contributions: Conceptualization, A.M.H.K., A.A.A., A.A., and M.B.C.; methodology, A.M.H.K.; software, A.M.H.K.; validation, A.M.H.K., A.A.A., and A.A.; formal analysis, A.M.H.K.; investigation, A.M.H.K. and A.A.A.; writing—original draft preparation, A.M.H.K. and A.A.A.; writing—review and editing, A.A.A. and A.A.; visualization, A.M.H.K.; project administration, M.B.C. All authors have read and agreed to the published version of the manuscript.

Funding: This research received no external funding.

Institutional Review Board Statement: Not applicable.

Informed Consent Statement: Not applicable.

Data Availability Statement: The original contributions presented in this study are included in the article. Further inquiries can be directed to the corresponding author.

Conflicts of Interest: The authors declare no conflicts of interest.

Abbreviations

The following abbreviations are used in this manuscript:

LFC	Load frequency control
UCFD	Unified control and fault diagnosis framework
min	Minimum value
$\Re$	Real part of an imaginary number
ISE	Integral squared error criterion
ISCE	Integral squared control effort
max	Maximum value

Appendix A. Derivation of the Feedforward Gain Q

Consider the linear time-invariant state-space representation of the system:

$$\dot{\mathbf{x}} = \mathbf{A}\mathbf{x} + \mathbf{B}u + \mathbf{B_d}\Delta P_L \tag{A1}$$

$$y = \mathbf{C}\mathbf{x} \tag{A2}$$

where $\mathbf{x} \in \mathbb{R}^n$ is the state vector, $u \in \mathbb{R}$ is the control input, $y \in \mathbb{R}$ is the system output, and $\Delta P_L \in \mathbb{R}$ is the load disturbance. The matrices $\mathbf{A}$, $\mathbf{B}$, $\mathbf{C}$, and $\mathbf{B_d}$ have compatible dimensions.

The control law incorporates state feedback and a feedforward term based on the observer signal r

$$u = -\mathbf{K}\hat{\mathbf{x}} - Qr \tag{A3}$$

Assuming the observer produces an asymptotically unbiased estimate of the state variables ($\hat{\mathbf{x}} \to \mathbf{x}$), the control law simplifies to

$$u = -\mathbf{K}\mathbf{x} - Qr \tag{A4}$$

Substituting (A4) into the system Equation (A1) yields the closed-loop state dynamics:

$$\dot{\mathbf{x}} = \mathbf{A}\mathbf{x} + \mathbf{B}(-\mathbf{K}\mathbf{x} - Qr) + \mathbf{B_d}\Delta P_L \tag{A5}$$

$$\dot{\mathbf{x}} = (\mathbf{A} - \mathbf{B}\mathbf{K})\mathbf{x} - \mathbf{B}Qr + \mathbf{B_d}\Delta P_L \tag{A6}$$

At steady state, the time derivatives vanish ($\dot{\mathbf{x}} = 0$). Let $\mathbf{x}_{ss}$, r_{ss}, and y_{ss} denote the steady-state values. From (A6), we have

$$0 = (\mathbf{A} - \mathbf{B}\mathbf{K})\mathbf{x}_{ss} - \mathbf{B}Qr_{ss} + \mathbf{B_d}\Delta P_L \tag{A7}$$

Solving for the steady-state state vector $\mathbf{x}_{ss}$,

$$\mathbf{x}_{ss} = (\mathbf{A} - \mathbf{B}\mathbf{K})^{-1}[\mathbf{B}Qr_{ss} - \mathbf{B_d}\Delta P_L] \tag{A8}$$

The primary design objective is to eliminate the steady-state output error, meaning $y_{ss} = \mathbf{C}\mathbf{x}_{ss} = 0$. Applying this constraint to (A8),

$$0 = \mathbf{C}(\mathbf{A} - \mathbf{B}\mathbf{K})^{-1}[\mathbf{B}Qr_{ss} - \mathbf{B_d}\Delta P_L] \tag{A9}$$

By distributing the $\mathbf{C}(\mathbf{A} - \mathbf{B}\mathbf{K})^{-1}$ term and rearranging to isolate the term containing Q, the following is obtained

$$\mathbf{C}(\mathbf{A} - \mathbf{B}\mathbf{K})^{-1}\mathbf{B}Qr_{ss} = \mathbf{C}(\mathbf{A} - \mathbf{B}\mathbf{K})^{-1}\mathbf{B_d}\Delta P_L \tag{A10}$$

The observer signal r at steady-state, driven by the disturbance ΔP_L through the observer error dynamics $(\mathbf{A} - \mathbf{L}\mathbf{C})$, is given by

$$r_{ss} = -\mathbf{C}(\mathbf{A} - \mathbf{L}\mathbf{C})^{-1}\mathbf{B_d}\Delta P_L \tag{A11}$$

Substitution of (A11) into the output constraint, Equation (A10), yields

$$\mathbf{C}(\mathbf{A} - \mathbf{B}\mathbf{K})^{-1}\mathbf{B}Q\big[-\mathbf{C}(\mathbf{A} - \mathbf{L}\mathbf{C})^{-1}\mathbf{B}_d\Delta P_L\big] = \mathbf{C}(\mathbf{A} - \mathbf{B}\mathbf{K})^{-1}\mathbf{B_d}\Delta P_L \tag{A12}$$

Assuming a non-zero disturbance ($\Delta P_L \neq 0$), canceling ΔP_L from both sides gives

$$-\big[\mathbf{C}(\mathbf{A} - \mathbf{B}\mathbf{K})^{-1}\mathbf{B}\big]\big[\mathbf{C}(\mathbf{A} - \mathbf{L}\mathbf{C})^{-1}\mathbf{B_d}\big]Q = \mathbf{C}(\mathbf{A} - \mathbf{B}\mathbf{K})^{-1}\mathbf{B_d} \tag{A13}$$

Because the system is single-input, single-output (SISO), the terms $\mathbf{C}(\mathbf{A} - \mathbf{B}\mathbf{K})^{-1}\mathbf{B}$ and $\mathbf{C}(\mathbf{A} - \mathbf{L}\mathbf{C})^{-1}\mathbf{B_d}$ evaluate to scalars. Dividing both sides by those scalars yields the final closed-form expression for the feedforward gain Q as

$$Q = -\frac{\mathbf{C}(\mathbf{A} - \mathbf{B}\mathbf{K})^{-1}\mathbf{B_d}}{[\mathbf{C}(\mathbf{A} - \mathbf{B}\mathbf{K})^{-1}\mathbf{B}] \cdot [\mathbf{C}(\mathbf{A} - \mathbf{L}\mathbf{C})^{-1}\mathbf{B_d}]} \tag{A14}$$

Appendix B. Selection of the Time Constant τ_Q

The residual signal is generated by the observer error dynamics of (34) as

$$\dot{\mathbf{e}} = (\mathbf{A} - \mathbf{LC})\mathbf{e} + \mathbf{B_d}\Delta P_L$$

Consequently, the transient component of the residual generator is not governed by the poles of $(\mathbf{A} - \mathbf{LC})$ but rather the dominate pole, which is written as

$$\min |\Re(\lambda(\mathbf{A} - \mathbf{LC}))|$$

Since the observer transient response decays almost completely after approximately five time constants, the parameter α is selected to be at least 5. Consequently, the auxiliary feedback controller remains effectively inactive during the observer transient, ensuring that the residual signal is primarily influenced by the disturbance and sensor fault rather than observer estimation errors. This establishes a clear time-scale separation between the observer and the auxiliary feedback controller dynamics.

References

1. Younis, W.; Yameen, M.Z.; Junejo, A.K.; Abido, M.A.; Khalid, M. Robust load frequency control in renewable integrated Multi Area grids using hybrid SA and QIO tuned PIDF controller. *Sci. Rep.* **2025**, *15*, 36848. [CrossRef]
2. Oladipo, S.; Sun, Y.; Adegoke, S.A. Application of soft computing techniques to load frequency control system of electric power systems: A brief survey. *Cogent Eng.* **2025**, *12*, 2572297. [CrossRef]
3. Yusuf, S.S.; Kunya, A.B.; Abubakar, A.S.; Salisu, S. Review of load frequency control in modern power systems: A state-of-the-art review and future trends. *Electr. Eng.* **2025**, *107*, 5823–5848. [CrossRef]
4. Sekyere, Y.O.; Effah, F.B.; Okyere, P.Y. Fractional order ANFIS controllers for LFC in RES integrated three-area power system. *J. Electr. Syst. Inf. Technol.* **2025**, *12*, 10. [CrossRef]
5. Fathy, A.; Bouaouda, A.; Hashim, F.A. A novel modified Cheetah Optimizer for designing fractional-order PID-LFC placed in multi-interconnected system with renewable generation units. *Sustain. Comput. Inform. Syst.* **2024**, *43*, 101011. [CrossRef]
6. Satapathy, P.; Mohanty, P.K.; Nayak, J.R.; Debnath, M.K.; Sahu, B.K.; Bajaj, M.; Bereznychenko, V.; Touti, E. Load frequency control of a PV–DSTS integrated thermal–hydro power system using a CCSA-optimized fuzzy fractional-order parallel controller. *Sci. Rep.* **2026**, *16*, 18630. [CrossRef]
7. Masikana, S.; Sharma, G.; Sharma, S.; Bokoro, P.N.; Çelik, E. Solar PV focused LFC studies utilizing an SFS-optimized PID with fractional derivative (PIDDμ), and incorporating BESS and FESS applications. *e-Prime Adv. Electr. Eng. Electron. Energy* **2024**, *10*, 100787. [CrossRef]
8. Nandanwar, S.R.; Patidar, N.P.; Panda, S.; Thakkar, J.; Kolhe, M.L. Synergistic control for enhancing frequency stability in grid-integrated network with decentralized renewable energy resources, energy storage, and electric vehicles. *Clean. Eng. Technol.* **2024**, *20*, 100757. [CrossRef]
9. Ewais, A.M.; Elnoby, A.M.; Mohamed, T.H.; Mahmoud, M.M.; Qudaih, Y.; Hassan, A.M. Adaptive frequency control in smart microgrid using controlled loads supported by real-time implementation. *PLoS ONE* **2023**, *18*, e0283561. [CrossRef]
10. Davoudkhani, I.F.; Zare, P.; Abdelaziz, A.Y.; Bajaj, M.; Tuka, M.B. Robust load-frequency control of islanded urban microgrid using 1PD-3DOF-PID controller including mobile EV energy storage. *Sci. Rep.* **2024**, *14*, 13962. [CrossRef]
11. El-Hameed, M.A.; Saeed, M.; Kabbani, A.; Abd El-Hay, E. Efficient load frequency controller for a power system comprising renewable resources based on deep reinforcement learning. *Sci. Rep.* **2025**, *15*, 18379. [CrossRef]
12. Liu, X.; Jiao, Q.; Yan, Z. Load frequency control with deep reinforcement learning under adversarial attacks. In *Proceedings of the 2023 IEEE 18th Conference on Industrial Electronics and Applications (ICIEA)*; IEEE: Piscataway, NJ, USA, 2023; pp. 257–262.
13. Chen, P.; Wang, W.; Fang, F.; Liu, J.; Chen, Z. A novel load frequency control strategy for renewable energy power system by coordinating energy storage and thermal power. *J. Energy Storage* **2025**, *108*, 115052. [CrossRef]
14. Trinh, D.T.; Wu, Y.K.; Pham, M.H. A novel load frequency control strategy for a modern power system by considering state-space modeling and stability analysis. *IEEE Access* **2024**, *12*, 115085–115101. [CrossRef]
15. Esmaeili, Z.; Heydari, H. Introducing a Novel Controller for Combined Load Frequency Control and Automatic Voltage Regulation of Interconnected Microgrids. *IET Renew. Power Gener.* **2025**, *19*, e70125. [CrossRef]
16. Magdy, G.; Bakeer, M.; Albalawi, H.; Zaid, S.A.; Bakeer, A. An accurate model of SMES for load frequency control in renewable power systems. *Ain Shams Eng. J.* **2025**, *16*, 103646. [CrossRef]
17. Tran, A.T.; Van Huynh, V.; Tran, T.L.T. Load Frequency Control Design for Complex Power Systems Implementing Integral Single-Phase Sliding Mode Control. *Eng. Technol. Appl. Sci. Res.* **2025**, *15*, 19802–19808. [CrossRef]

18. Tran, A.T.; Van Huynh, V.; Shim, J.W.; Lim, C.P. Optimized sliding mode frequency controller for power systems integrated energy storage system with droop control. *IEEE Access* **2025**, *13*, 43749–43766. [CrossRef]
19. Shayeghi, H.; Rahnama, A.; Bizon, N. Green microgrid's LFC using recursive step-by-step optimized multi-stage fuzzy controller with separated inference systems. *Renew. Energy Focus* **2024**, *51*, 100625. [CrossRef]
20. Tran, A.T.; Van Huynh, V.; Nguyen, B.L.H.; Shim, J.W.; Do, T.D. Multi-stage sliding mode control design with optimal state estimator for load frequency regulation in hybrid-source power systems. *Sci. Rep.* **2025**, *15*, 43795. [CrossRef]
21. Tran, A.T.; Duong, M.P.; Pham, N.T.; Shim, J.W. Enhanced sliding mode controller design via meta-heuristic algorithm for robust and stable load frequency control in multi-area power systems. *IET Gener. Transm. Distrib.* **2024**, *18*, 460–478. [CrossRef]
22. Ahmed, E.B.; Attia, M.A.; Hamouda, R. Load Frequency Control of Single Area Using New Adaptive Controller. In *Proceedings of the 2024 25th International Middle East Power System Conference (MEPCON)*; IEEE: Piscataway, NJ, USA, 2024; pp. 1–6.
23. Zhao, Y. Reinforcement Learning Data-Driven Optimal Load-Frequency Control for Power Systems. *EAI Endorsed Trans. Energy Web* **2024**, *12*. [CrossRef]
24. Du, W.; Huang, X.; Zhu, Y.; Wang, L.; Deng, W. Deep reinforcement learning for adaptive frequency control of island microgrid considering control performance and economy. *Front. Energy Res.* **2024**, *12*, 1361869. [CrossRef]
25. Guo, W.; Du, H.; Han, T.; Li, S.; Lu, C.; Huang, X. Learning-driven load frequency control for islanded microgrid using graph networks-based deep reinforcement learning. *Front. Energy Res.* **2024**, *12*, 1517861. [CrossRef]
26. Hassan, A.; Aly, M.; Selim, A.; Elmelegi, A.; Aldhaibani, A.; Mohamed, E. Optimal cascade 2DOF fractional order master-slave controller design for LFC of hybrid microgrid systems with EV charging technology. *Results Eng.* **2025**, *25*, 103647. [CrossRef]
27. Shen, Z.; Chen, G. Robust H_∞ control for LFC of discrete T–S fuzzy MAPS with DFIG and time-varying delays. *J. Comput. Appl. Math.* **2025**, *457*, 116271. [CrossRef]
28. Wang, Y.; Xi, Z.; Zhang, B.; Zhang, T.; He, C. Resilient Event-Triggered Hinf Control for a Class of LFC Systems Subject to Deception Attacks. *Electronics* **2025**, *14*, 2713. [CrossRef]
29. Guo, D.T.; Zhao, Y.X.; Shi, K.B.; Zhu, M. Dynamic Event-Triggered Switching of LFC Scheme Under DoS Attacks Based on a Predictive Model. *Electronics* **2025**, *14*, 2838. [CrossRef]
30. Xianchuan, D.S.; Linlin, L.; Bin, J. Unified control and detection framework and its applications: A review, some new results, and future perspectives. *J. Syst. Eng. Electron.* **2021**, *32*, 995–1013. [CrossRef]
31. Saadat, H. *Power System Analysis*; McGraw-Hill: New York, NY, USA, 1994.
32. Deng, X.; Bian, D.; Shi, D.; Yao, W.; Wu, L.; Liu, Y. Impact of low data quality on disturbance triangulation application using high-density PMU measurements using high-density PMU data. *IEEE Acc.* **2019**, *7*, 105054–105061. [CrossRef]
33. Bevrani, H. *Robust Power System Frequency Control*; Springer: Berlin/Heidelberg, Germany, 2014.
34. Nagsarkar, T.; Sukhija, M. *Power Systems Analysis*; OUP India: New Delhi, India, 2007.
35. Franklin, G.F.; Powell, J.D.; Emami-Naeini, A. *Feedback Control of Dynamic Systems*; Pearson: London, UK, 2025.
36. Glad, T.; Ljung, L. *Control Theory*; CRC Press: Boca Raton, FL, USA, 2000.
37. Ding, S.X. *Model-Based Fault Diagnosis Techniques: Design Schemes, Algorithms, and Tools*; Springer: Berlin/Heidelberg, Germany, 2013.
38. Skogestad, S.; Postlethwaite, I. *Multivariable Feedback Control: Analysis and Design*; John Wiley & Sons: Hoboken, NJ, USA, 2005.

Disclaimer/Publisher's Note: The statements, opinions and data contained in all publications are solely those of the individual author(s) and contributor(s) and not of MDPI and/or the editor(s). MDPI and/or the editor(s) disclaim responsibility for any injury to people or property resulting from any ideas, methods, instructions or products referred to in the content.